CR-44
TU-42345
P-88

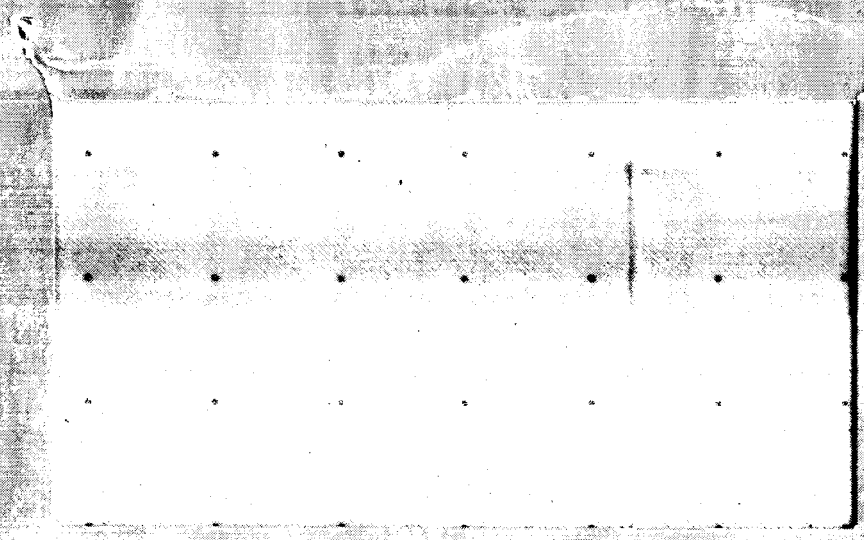

DTM-79-1

CONCEPTUAL DESIGN OF AN OPEN CYCLE AIR BRAYTON SOLAR RECEIVER

PHASE I FINAL REPORT

by
Walter B. Bienert
Harold Rind
David A. Wolf

January 15, 1979

Prepared under Contract No. 955135

for

California Institute of Technology
Jet Propulsion Laboratory

by

Dynatherm Corporation
One Industry Lane
Cockeysville, Maryland

FOREWORD

This report documents the results of a conceptual design study for an Open Cycle Air Brayton Solar Receiver. The work was initiated on July 6, 1978 and completed on January 15, 1979. One of the requirements of the study was the preparation of a proposal for the final design and development of a prototype receiver. This proposal is being submitted as a separate volume.

The program was undertaken by Dynatherm for JPL. Dr. Walter Bienert served as Dynatherm's Program Manager and Mr. David A. Wolf as Project Engineer. JPL's Technical Monitor for the study was Mr. William A. Owen. The authors of the report gratefully acknowledge his cooperation and guidance throughout the program.

TABLE OF CONTENTS

1. INTRODUCTION

Solar thermal power systems collect solar energy and heat a working fluid for operation of a heat engine. The heat engine is then coupled to a generator to produce electricity. Within this framework, a specific technology is that of distributed, point focusing power systems of small individual power capacity. These systems involve a tracking paraboloidal dish concentrator with the heat receiver mounted at the focus and the engine mounted at the focus or the ground. Typical power levels for these systems are 50 to 100 kW of solar input and 15 to 20 kW of electrical output.

This report describes the results of a Phase 1 study concerning the heat receiver of a distributed small power system. The specific objective was the conceptual design of a receiver for an open cycle, air Brayton engine (Air Brayton Solar Receiver, ABSR). The design point and the performance goals for the ABSR were specified by JPL and are summarized in Table 1.1. The receiver will be mounted at the focal point of an 11 m concentrator, and the Brayton Cycle Power Conversion Unit (PCU) will be attached directly to the receiver. In order to accommodate short term transients such as clouds, provisions for heat from buffer storage for a ten minute interval are included in the design.

Reference 1 states a cost goal for the ABSR of 30 $/kWe for 1982 and 20 $/kWe for 1985. For a 15 kWe system, the corresponding receiver cost goals are $450 and $300, respectively. Obviously, such goals can be achievable only in very large quantity productions where most labor costs are eliminated through automation. There is some doubt, however, whether the above goals are realistic in any production quantity. At the present time, there is no precedence for solar receiver manufacture and marketing practice. But some guidelines can be obtained from related products which are currently produced and marketed in very large quantities. Examples of such products are air duct heaters, heat exchangers and evaporator, and condenser coils of HVAC equipment. These randomly selected examples have the common denominator that they exchange heat with an airstream and that they are also rates in terms of thermal

Ref. 1: Point Focusing Distributed Receiver Technology Project Annual Technical Report, Fiscal Year 1978, prepared by Jet Propulsion Laboratory

TABLE 1.1

RECEIVER DESIGN POINT AND PERFORMANCE GOALS

Peak Thermal Input	85 kW
Peak Solar Flux at Aperture	$\sim 1.5 \times 10^7$ W/m^2
Air Inlet Temperature	565°C
Air Outlet Temperature	815°C
Receiver Inlet Pressure	0.25 MPa
Air Mass Flow Rate	0.24 kg/sec
Pressure Drop: Goal	2%
Maximum	4%
Thermal Efficiency: Short Term Goal	80%
Long Term Goal	85%

power, i.e., kilowatts or Btu/hr. A survey of industrial catalogues revealed that their selling prices (prorated to 85 kWth) ranges from about 1000 to 2000 dollars. Considering that the above mentioned products generally use low alloy steel as the prevalent component, while a 800°C solar receiver must, by necessity, utilize more expensive materials, a reasonable cost bogey appears to be toward the upper end of the above price range.

A similar conclusion can be drawn from the selling price per weight ratio of typical, mass produced industrial products. Examples are consumer products such as engines, refrigerators, lawn mowers, air-conditioners, etc., the ratio is $1.50 per pound; industrial machinery (drill presses, lathes, etc.) is $1.80 per pound; and heat exchange equipment is approximately 2 to 4 dollars per pound. Since the weight of a solar receiver for 85 kWth is probably going to be in the 500 to 1000 pound range, the above examples suggest again a probable selling price in the 1000 to 2000 dollar range.

The preceding discussion is not intended to prejudge the cost of an ABSR in mass production. The ultimate cost can only be determined after the design is completed and, most of all, after it has been engineered for mass production. Initial and admittedly very rough estimates indicate that a cost goal of about 1000 dollars or $70 per kWe might be achievable.

2. SUMMARY OF ABSR DESIGN

The baseline design of the ABSR as it evolved from the Phase 1 study is shown in Figures 2.1 and 2.2. Air from the recuperator enters the ABSR at the top and is distributed by the inlet plenum to 19 individual heat exchangers. The latter are attached to liquid metal heat pipes which form a "curtain wall" inside the cavity. The heated air is collected near the bottom of the ABSR in a torus and then is ducted toward the turbine of the PCU. Each of the heat pipes contains a latent heat storage capsule which provides sufficient buffer storage for a ten minute solar outage.

The main feature of this design are the liquid metal heat pipes. The primary function of the heat pipes is to diffuse the concentrated solar flux nearly loss free to a flux level which is more compatible with metal-to-gas heat transfer. The internal heat transfer coefficient in a liquid metal heat pipe is typically in the order of 5000 Btu/hr-ft^2-^{o}F (30,000 W/m^2-^{o}C) as compared to 50 Btu/hr-ft^2-^{o}F (300 W/m^2-^{o}C) for heat transfer to gases. Because of these high coefficients, the ΔT's between the metal and the fluid are reduced to almost negligible values. Conversely, the heat pipe can accept very high heat fluxes without incurring large temperature differences. Furthermore, the energy is transported within the heat pipe in the form of latent heat, thus the transport occurs nearly isothermally.

These features of the heat pipe lead to several important advantages in an ABSR. They are:

1. Since the heat pipe can tolerate higher solar fluxes than a direct solar radiation-to-gas heat exchanger, the receiver can be made more compact. The flux on the cylindrical wall of the cavity diminishes with increasing radius. The heat pipes may be located at a smaller radius than a conventional heat exchanger which results in a smaller overall receiver diameter and thus in lower convective losses from the insulation.

2. The flux transformation afforded by the heat pipes leads to either lower metal temperatures or lower pressure drops. The two are interdependent through the Reynolds analogy which relates the heat transfer coefficient and the friction coefficient in a gas. A brief comparison between a heat pipe and a conventional heat exchanger has shown that for the same pressure drop the maximum metal temperatures would be about 100^{o}C higher in the conventional heat exchanger (even when located at nearly

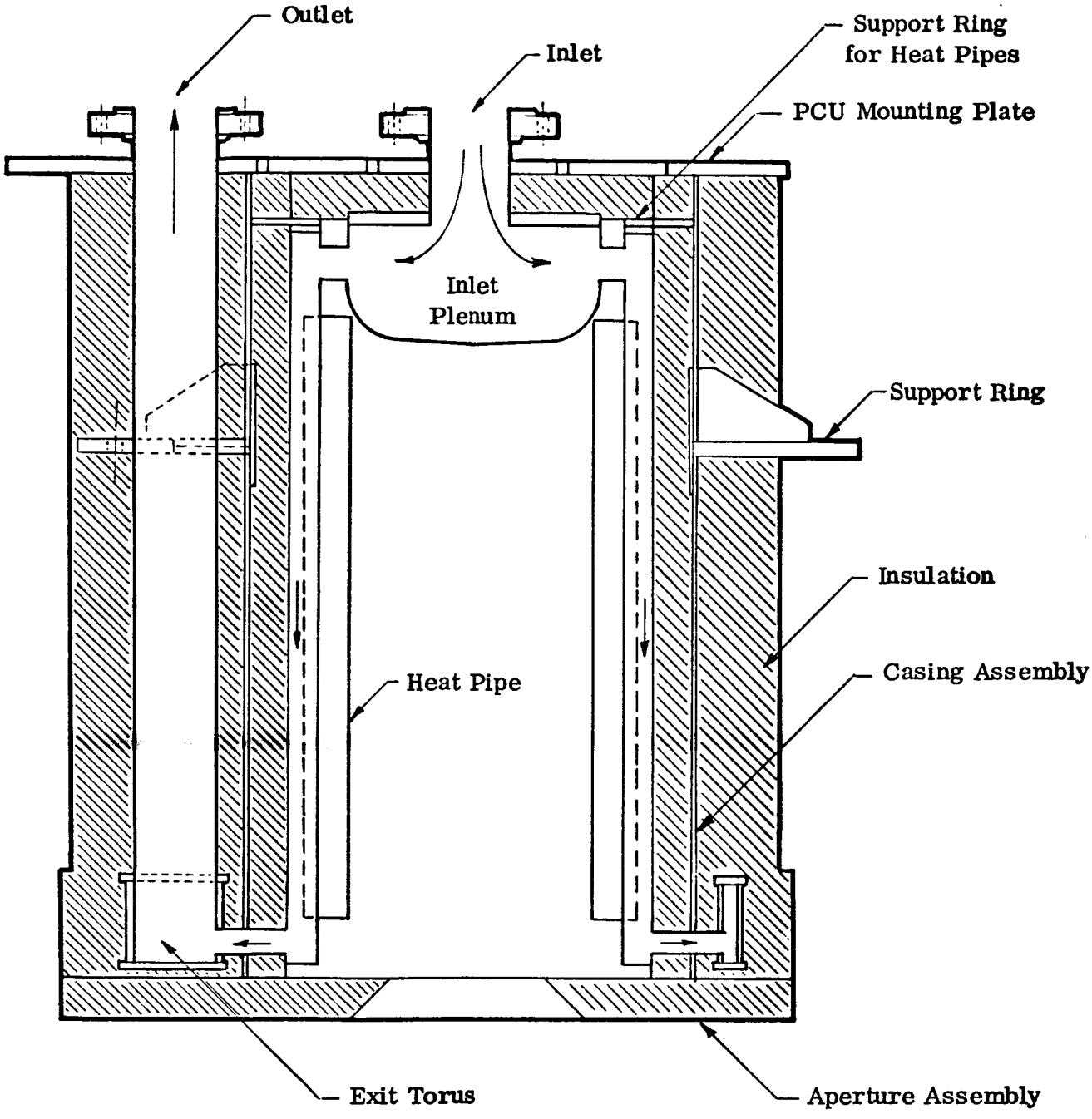

FIGURE 2.1

SCHEMATIC OF HEAT PIPE ABSR

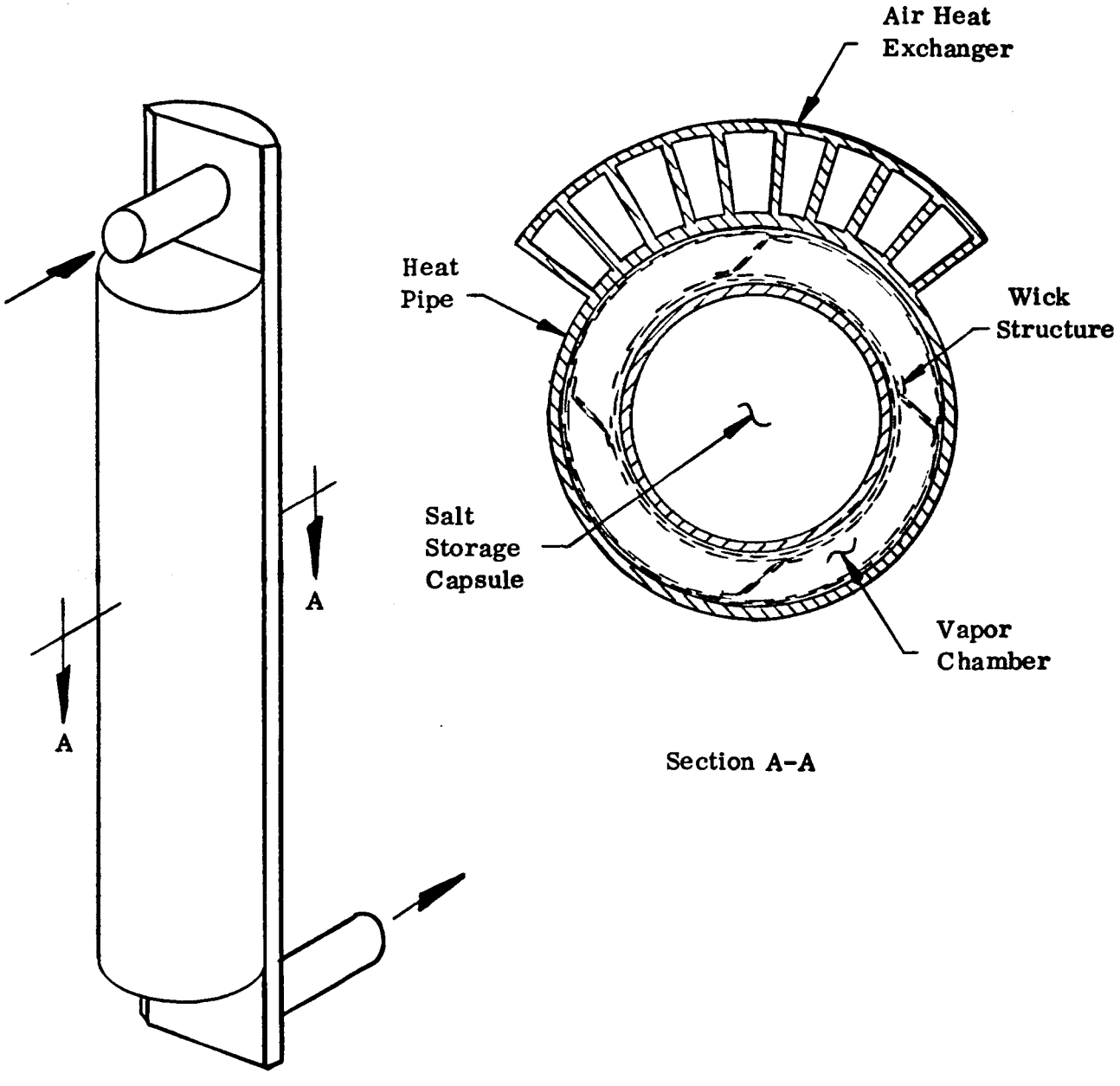

FIGURE 2.2

SCHEMATIC OF HEAT PIPE HEAT EXCHANGER

twice the radius of the heat pipe receiver). Conversely, if designed for the same metal temperature, the conventional design would incur a 2.72 kPa higher pressure drop. The penalty for this ΔP at design output is about 0.71 kW of compressor power or 4.2% of the thermal input to the receiver.

3. The high heat transfer coefficient of the heat pipes permits design for a higher solar flux. It also makes the system tolerant to flux excursions which might occur as a result of misalignment of the receiver with respect to the concentrator. At the nominal design point, the maximum ΔT between the flux absorbing surface and the working fluid is approximately $35^{o}C$, while in a conventional receiver the corresponding ΔT is about $220^{o}C$. Doubling the flux, for instance, would have little effect on the heat pipe receiver but would cause excessive metal temperatures in a conventional receiver.

4. Another important asset of the heat pipe design is that the thermal storage material is located within the vapor space of the heat pipe. This location provides a thermally ideal environment. The same high heat transfer coefficient which proves so beneficial at the evaporator applies also to the storage medium. Heat can be withdrawn with little loss in temperature which is important for high engine efficiency. The location of the storage material within the heat pipes causes no additional pressure drops and no valving or rerouting of the fluid is required.

5. Finally, the heat pipe design has ample growth potential. The current design, without modifications (except possibly enlarging the aperture), can handle net input powers of up to 135 kWth and would still meet the specified pressure drop and would not exceed allowable metal temperatures and stresses. The design can also be adapted to other types of conversion systems. In fact, it is almost mandatory for a solar receiver with a Stirling engine.

Although the development cost may be somewhat higher than for a receiver using conventional heat exchanger technology, its inherent advantages, its adaptability, and growth potential argue that it be carried into the next phase of the development.

A performance summary of the heat pipe ABSR is given in Table 2.1. The performance data apply for the specified mass flow rate of 0.242 kg/sec which corresponds to a net thermal input of 68 kW. A summary of the critical materials is given in Table 2.2. Type 310 stainless steel is employed in the high temperature zones of the receiver. The ducts carrying the $816^{o}C$ air stream will be fabricated

TABLE 2.1

HEAT PIPE ABSR PERFORMANCE SUMMARY
(DESIGN POINT)

Design Power	68.6 kW
Air Flow Rate	0.24 Kg/sec (0.533 lb/sec)
Air Inlet Temperature	$566^{o}C$ ($1050^{o}F$)
Air Exit Temperature	$816^{o}C$ ($1500^{o}F$)
Maximum Cavity Temperature	$906^{o}C$ ($1662^{o}F$)
Peak Flux on Receiver Surface	330 kW/m^2 (10^5 $Btu/hr-ft^2$)
Receiver Efficiency*	0.88
Pressure Loss	2.56 KPa (0.372 psi)
Total Weight	496 Kg (1093 lbs)
Operating Time from Storage**	13.7 minutes

*Based on Wind Speed of 16.1 km/hr (10 mph)
**Down to 25% of Design Power

TABLE 2.2

RECEIVER MATERIAL SUMMARY

Heat Pipe Envelope	310 Stainless Steel
Wick Structure	304 Stainless Steel
Working Fluid	Sodium
Heat Exchanger	310 Stainless Steel
Buffer Storage	LiF_2-MgF_2
Inlet Duct and Manifold	Low Alloy Steel (1% Chromium, $\frac{1}{2}$% Molybdenum)
Outlet Duct and Manifold	304 Stainless Steel
Receiver Structure	Hot and Cold Rolled Steel
Insulation	Cerablanket*, Microlite**
Aperture	Cera Form Board*

*Aluminum-Silica Ceramic Fiber, Johns-Manville
**Borasilicate Glass Fiber, Johns-Manville

from the less expensive type 304 stainless steel, while all other components utilize inexpensive low alloy or carbon steel.

The development of the ABSR is foreseen to occur in three progressive phases. The first phase is the development, fabrication, and testing of one or several prototypes. These will be almost identical to the design generated during Phase 1. The fabrication process will follow established heat pipe fabrication techniques which were developed for use in laboratories. No significant new tooling or automation is expected during this phase. The main purpose of this phase is demonstration of the technical feasibility of the concept. In a few details, the prototypes will differ from the baseline design. Some of the preferred materials can only be obtained in "mill run" quantities, thus substitutions will have to be made. The preferred buffer storage material is $LiF-MgF_2$ eutectic which required Inconel 617 as a container. This alloy is not available in the required tubing form, although it certainly can be produced if sufficient quantities warrant the tooling up by the manufacturer. Therefore, sensible heat storage of pure iron will be substituted for the latent heat storage of the salt. The storage capacity (based on the same volume) will be reduced by only 16%, but a weight penalty of 185 pounds will occur.

The second phase of the development will be addressed to moderate production quantities of about 100 units annually. The same basic design with a few modifications to improve fabricability will be used. One modification is the substitution of a thin walled round torus for the heavy square torus in the current design. Tooling for a round torus is not warranted for prototype quantities. Other minor modifications to improve fabricability are also envisioned. The major change between prototypes and moderate production quantities will be the development of an improved and simplified heat pipe fabrication process. It is estimated that with a relatively small investment of about $200,000 the labor input can be reduced by a factor of ten (from currently about 10 hours per heat pipe to about one hour).

The final phase will be complete automation of the fabrication process and will be warranted for quantities of perhaps 10,000 or more annually. Automation will require a redesign of the ABSR in order to enable the use of mass production techniques.

Preliminary cost estimates for prototypes and for small and large production quantities are as follows:

Prototypes	$27,000
Small Quantities (~100)	$ 5,000
Large Quantities (>10,000)	$ 1,100 - $2,600

The estimates for the first two categories are based on a step-by-step fabrication plan and firm quotes for most materials. The estimate for the large quantities are by necessity much less firm. The higher figure of the indicated range was obtained by extrapolating material costs for the baseline design to very large quantities and then adding a labor cost of $1.23 per pound weight of the receiver. The lower figure was obtained in a different way. It is based on a preliminary estimate of labor and material cost of an advanced, integrated heat pipe-heat exchanger. Added to this was then the cost of 250 pounds of supporting structure and insulation at a rate of $1.50 per pound of fabricated material. Although these estimates for large production quantities are only very rough at the present time, they show that a heat pipe ABSR has the potential of approaching the cost goals set by the JPL program.

3. DESIGN CHOICES

The scope of the study encompassed the investigation of several design concepts for an ABSR. Additionally, a parametric study of receivers covering a wide range of input power levels, temperatures, and gas flow rates was performed.

An early ABSR concept is shown in Figures 3.1, 3.2, and 3.3. In this design, a cavity is formed by the evaporators of three concentric rings of heat pipes. The lengths of the evaporators increase progressively from the innermost to the outermost ring. The condenser sections of the heat pipes form three similar rings within a gas plenum above the evaporators. The air to be heated enters into a plenum surrounding the condensers and then passes radially inward over the finned condensers. The heated air then exits axially from the center of the receiver. The evaporators and condensers have different diameters in order to permit "close packing" within the cavity, yet provide room for fins and air passages in the gas plenum. As in the final design, capsules containing a fusible salt for buffer storage are located inside the evaporators of the heat pipes.

The advantage of this design is the low pressure drop associated with the simple, unobstructed gas passages. Unfortunately, this advantage is more than counterbalanced by the need for a large number of heat pipes (47). A large fraction of the expected receiver cost is associated with the fabrication and processing of the heat pipes. This may not be true for large quantity productions where everything is automated, but it certainly holds for prototypes and small production quantities. Thus the cost of this type of receiver is expected to be relatively high. (The design was abandoned before a detailed cost estimate was performed.) This concept also poses some difficult assembly problems. Because of the closeness of the heat pipes, the attachment and sealing to the pressure plate which separates the pressurized plenum from the cavity is very difficult. A further disadvantage is the high solar flux on the evaporator end caps of the heat pipes, at least on the inner two rows.

This concept of an ABSR would become more viable if the inner two rings of heat pipes could be eliminated. This would require rerouting of the gas over the heat exchanger, possibly in the form of a multipass arrangement as shown schematically

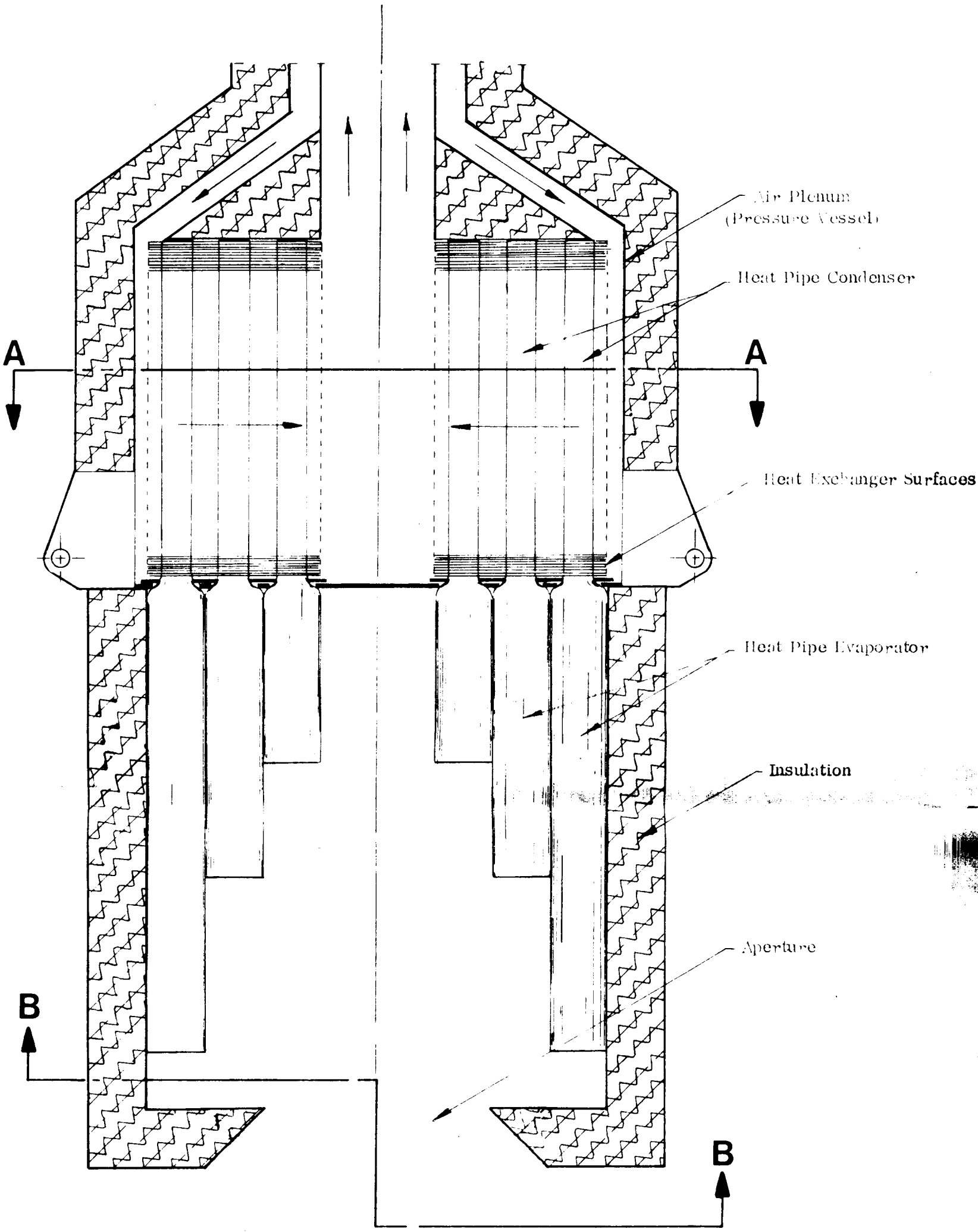

Figure 3-1
Layout of Air Brayton
Solar Receiver
Scale: 1/4"=1"

dynaTherm
CORPORATION

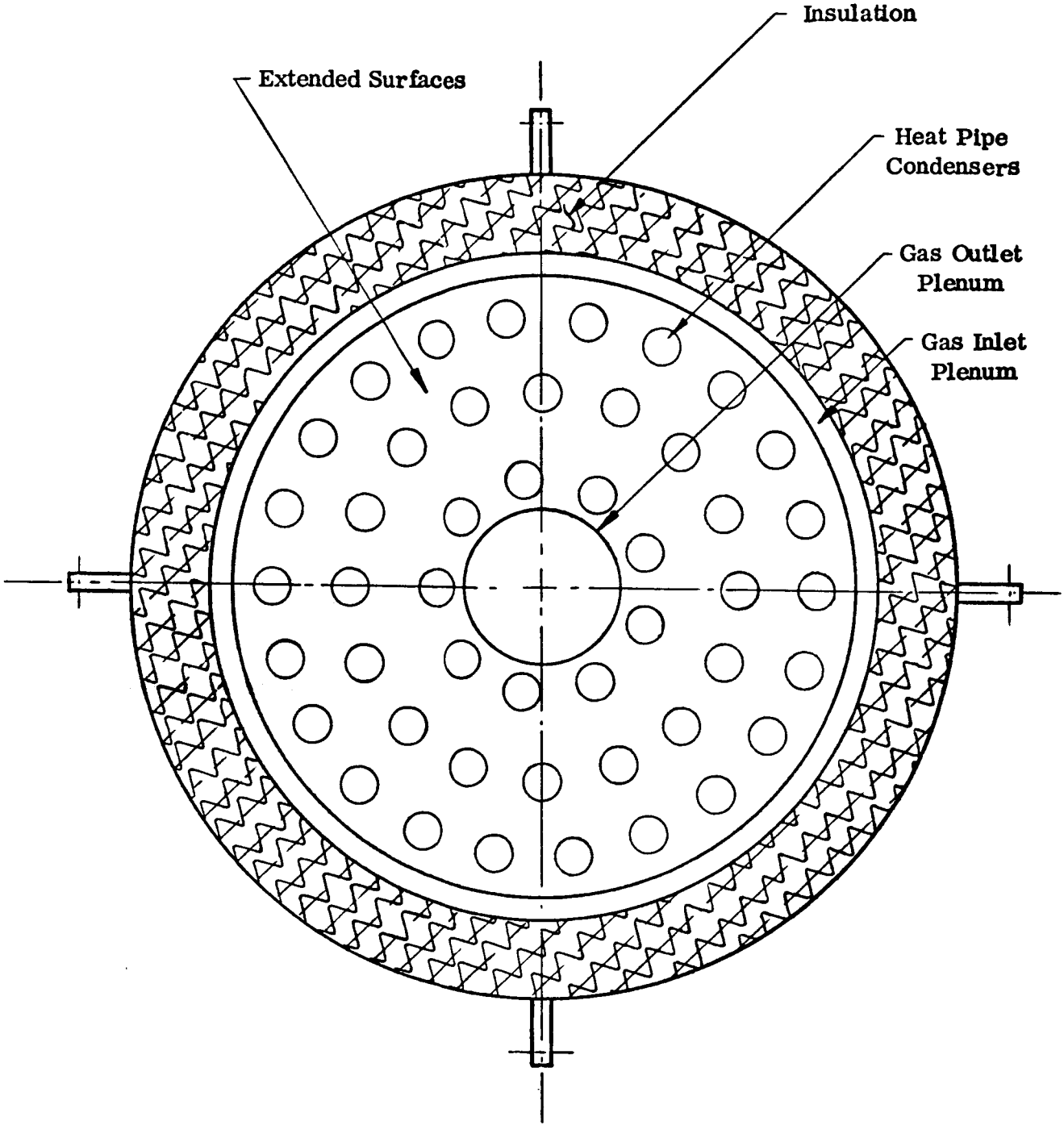

FIGURE 3.2

SECTION A-A

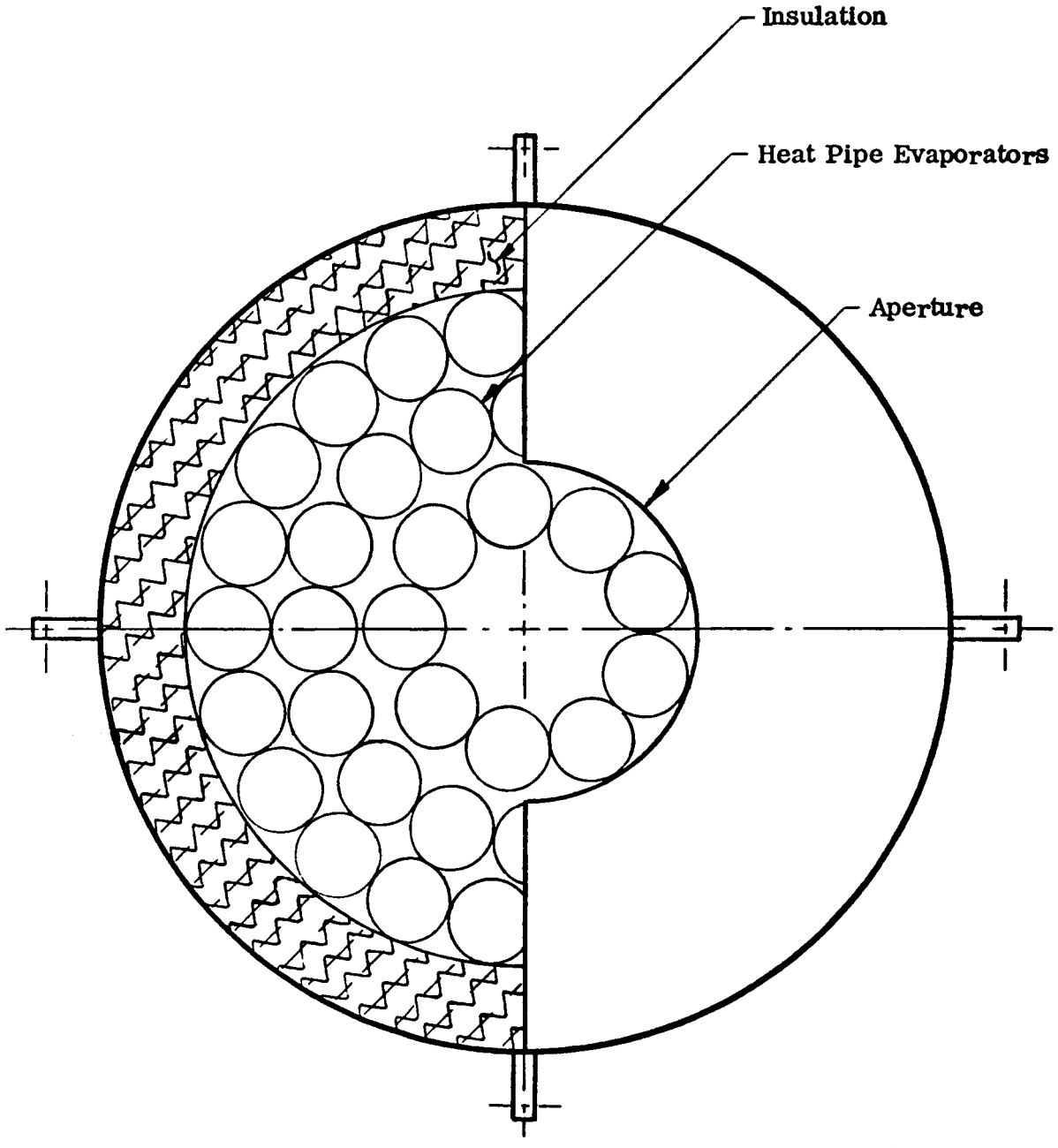

FIGURE 3.3

SECTION B-B

in Figure 3.4. Assuming a 30 cm long condenser with radial fins (3 fins per cm, 1.6 cm high on a 2.5 cm diameter tube), the available heat exchanger area would be comparable with that of the selected baseline design. Unfortunately, the time schedule and funding limitations did not permit a detailed evaluation of this alternate design.

The parametric study, which was conducted during early parts of the program, covered a wide range of operating conditions. These are listed in Table 3.1. The approach which was taken during the analysis was to select a single receiver geometry (the one shown in Figure 3.1) and to evaluate its performance for all specified conditions. In order to perform the analysis, the spatial distribution of the solar flux within the cavity had to be calculated. This was done for a 12.55 m diameter concentrator which collects about 90 kWt. For the other two input powers of 50 and 150 kWt, the spatial distribution was retained and only the magnitude of the flux was varied. This approach is only an approximation since different peak powers require concentrators of different diameters and, consequently, different spatial flux distributions. (The 50 kWt case is a correct representation of the 12.55 m concentrator if a reduced solar constant is assumed.) Despite these shortcomings, the analysis showed that the heat pipe receiver is very adaptable. One single geometry can handle solar inputs ranging from 50 to 150 kWt with an efficiency exceeding 80% and with pressure losses of less than 4% of the inlet pressure.

The parametric study also included the evaluation of various concepts for buffer storage. Both latent and sensible heat storage systems were studied. Table 3.2 lists five candidate salt mixtures whose melting points fall within the range of interest. During normal operation at the design point, the storage medium will be fully charged; i.e., the salt will be molten. The salt temperature will be nearly the same as the vapor temperature within the heat pipes. If the power conversion unit were to operate at constant turbine inlet temperature, only the latent heat of fusion could be made available as buffer storage output. Constant temperature operation would also require the selection of a design temperature which is only slightly above the melting point of the salt. On the other hand, if the turbine inlet temperature is allowed to drop while operating from storage, both sensible and latent heat is made available.

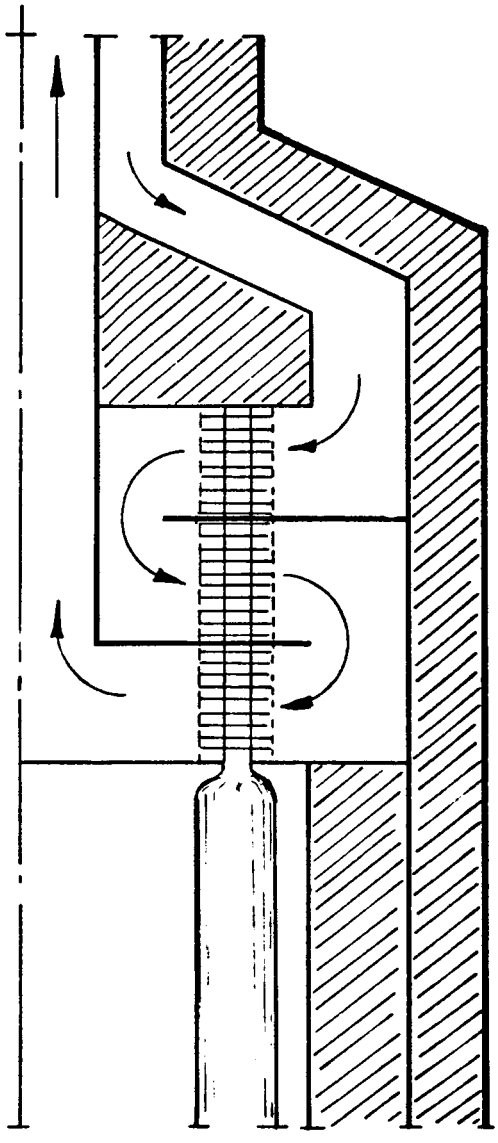

FIGURE 3.4

MULTIPASS HEAT EXCHANGER ARRANGEMENT
OF ALTERNATE DESIGN

PARAMETERS FOR THERMAL PERFORMANCE ANALYSIS								UNITS
Peak Thermal Power	50		90		150			kWt
(Corresponding Concentrator Diameter)	9.36		12.55		16.21			m
Fluid Outlet Temperature	538 1000		704 1300		816 1500		871 1600	^{o}C ^{o}F
Fluid Inlet Temperature	427 800		538 1000		593 1100		649 1200	^{o}C ^{o}F
Fluid Inlet Pressure	204 30		306 45		408 60		510 75	kPa psig
Specific Fluid Flow Rates	0.0082	0.0055	0.0041	0.0032	0.0027	0.0023	0.0018	kg/sec-kWt
(Corresponding Gas ΔT)	111	167	222	278	333	389	444	^{o}C

TABLE 3.1

MATRIX OF PARAMETERS FOR THERMAL PERFORMANCE ANALYSIS

Salt Mixture	Melting Point (°C)	Heat of Fusion W-hr/kg	Heat of Fusion W-hr/cm³	% ΔV on Fusion	Cost $/kW-hr(t)	Cost $/kg
$LiF-MgF_2$	741 ± 5	256	0.552	22.5*	35.3	9.01
$NaF-MgF_2$	832 ± 5	174	0.390	22.8	49.7	8.66
$Li_2O-B_2O_3$	650 ± 0	115	0.227			
$LiF-MgF_2-NaF$	632 ± 5	232	0.511	23.2*	38.6	8.96
$LiF-MgF_2-KF$	713 ± 5	263	0.569	22.6*	34.1	8.95

*Estimated from Components

TABLE 3.2

THERMOPHYSICAL PROPERTIES OF CANDIDATE EUTECTIC SALT MIXTURES

The monogram given in Figure 3.5 allows an estimate of the total availalbe heat as a function of initial and final salt temperature. As an example, $LiF-MgF_2$ when operated between 871 and 566°C (1600 and 1050°F) yields 171 Watt-hr/kg (265 Btu/lb) of sensible heat in addition to its latent heat of 255 Watt-hr/kg (396 Btu/lb). Of the five materials listed in Table 3.2, the eutectic oxide was eliminated because of insufficient property and compatibility data. Of the four fluoride salt mixtures, the two with the highest melting points, $LiF-MgF_2$ and $NaF-MgF_2$, were selected for more detailed study.

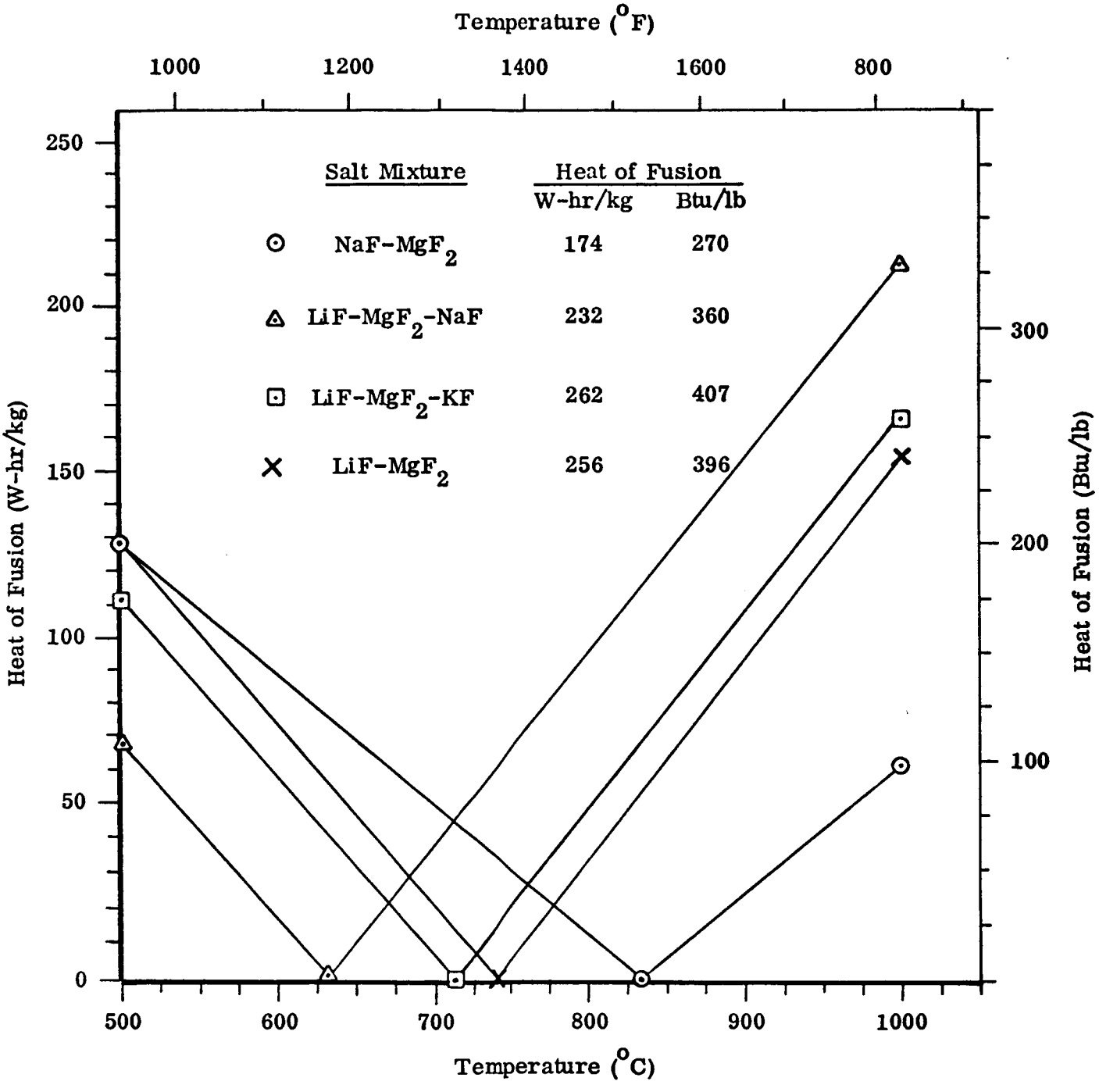

FIGURE 3.5

NOMOGRAM OF SENSIBLE HEAT OF FLUORIDE SALTS

4. THERMAL DESIGN AND PERFORMANCE

The performance of the baseline receiver design was evaluated at a variety of operating conditions. The steady-state performance of the receiver was characterized in terms of thermal efficiency and pressure drop at the design point and at reduced thermal inputs corresponding to 25% and 50% of the design value. In addition, the transient behavior of the receiver was evaluated during diurnal variations in solar insolation and during sudden interruptions due to cloud cover. The performance analysis also included the determination of the receiver's sensitivity to adverse operating conditions, such as those imposed by air flow interruption or receiver misalignment relative to the concentrator's focal point.

4.1 Design Point Performance

To facilitate the performance evaluation, the flux distribution within the receiver was determined using a computer program developed early in the program. Basically, this program is capable of predicting the incident flux on any surface which is either parallel or perpendicular to the receiver axis. The characteristics of the concentrator which are used in the model are summarized in Table 4.1. The concentrator was assumed to be divided in 1068 segments. Each segment was assumed to be a perfect concentrator, and the segment packing density was assumed to be 89%. To account for the concentrator slope error of 1 milliradian, the half angle of the sun was increased by 2 milliradians. The flux distributions predicted by this model agree quite well with the flux distributions provided by JPL.

Figure 4.1 summarized the predicted flux distribution within the receiver at the design point. Ninety-five percent of the energy which enters the cavity impinges directly on the cylindrical portions of the heat pipe evaporators. The remaining energy falls on the inlet plenum located at the top of the receiver. The peak flux within the receiver is 330 kW/m^2 and occurs 13 cm from the lower end of the heat pipe. The predicted fluxes on the inlet plenum are quite low and present no special design problems. Another important feature of the receiver flux distribution is that the heat pipe end caps are not directly illuminated. As a re-

TABLE 4.1

CONCENTRATOR CHARACTERISTICS

Diameter	11.02
Focal Length	6.61 m
Central Void Diameter	1.07 m
Reflectivity	0.86
Slope Error	1 milliradian
Packing Density of Reflector Segments	0.89

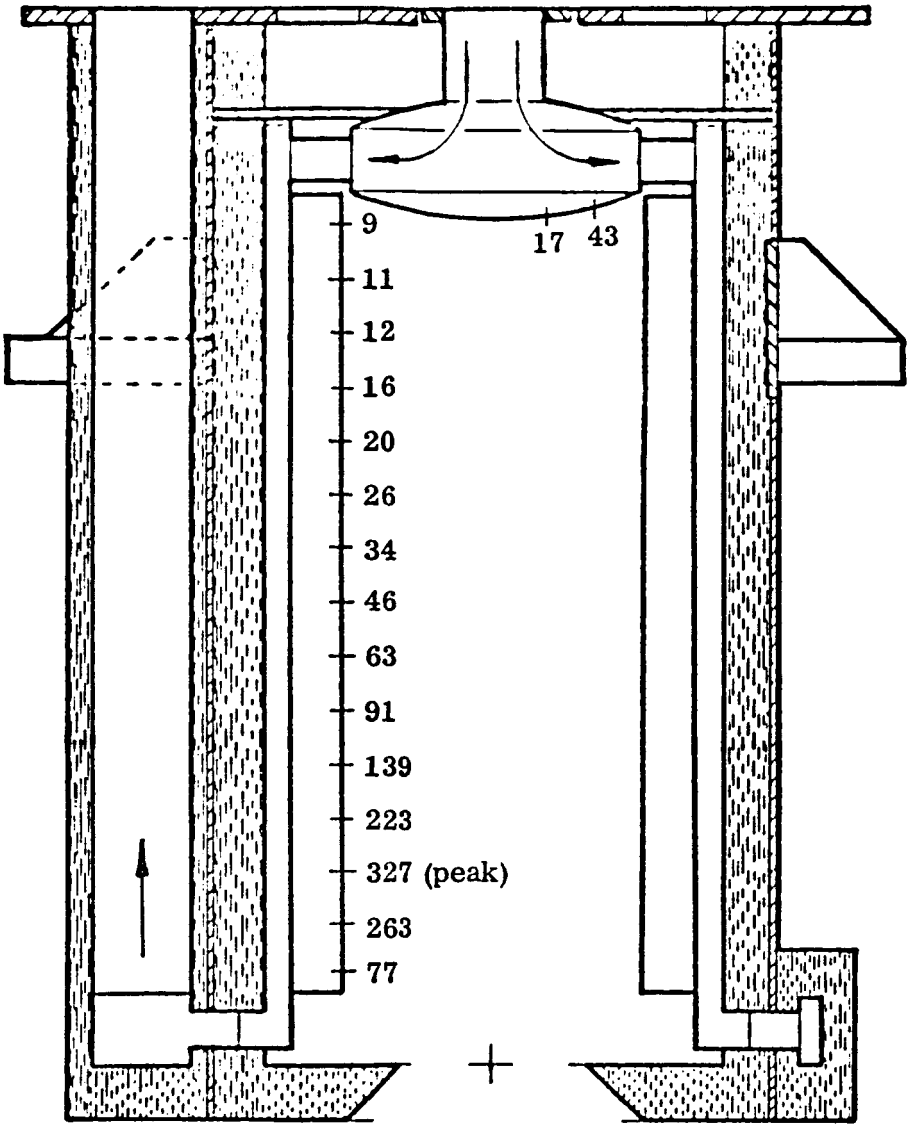

Note: All Fluxes in kW/m^2

FIGURE 4.1

FLUX DISTRIBUTION IN CAVITY

sult, the end caps need not be wicked surfaces which simplifies the design considerably.

At the design point, air enters the receiver at 565°C (1050°F) and exits at 816°C (1500°F). The design air flow rate is 0.24 kg/sec. Under these conditions and with the incident flux distribution shown in the previous figure, the temperatures at key locations within the receiver shown in Figure 4.2 were calculated. This temperature distribution is basically a function of the incident flux, the air flow rate, and the thermal resistance of the heat pipe. This resistance is determined by convective heat transfer within the air heat exchanger, fin effectiveness of the heat transfer surfaces, conduction through the heat pipe wall, and evaporation and condensation film coefficients within the heat pipe. The effects of radiation exchange between various points in the receiver was neglected except when the inlet plenum surface was determined. As a result, the peak temperature within the cavity will be slightly lower than shown in the figure.

The maximum cavity temperature occurs on the cylindrical portion of the heat pipe evaporator where the flux is highest and is 906°C. Temperatures at other points on the evaporator surface are fixed by the local flux and the heat pipe vapor temperature which is 873°C. The temperature of the air heat exchanger is 856°C at the upper end and 870°C at the lower end. This variation reflects the variation in the air temperature which gradually increases as the air moves toward the toroidal exit plenum at the bottom of the receiver. The air is directed downward through the heat exchanger to promote condensation preferentially at the upper end of the heat pipe. This assures gravity-assisted condensate return to the evaporator surface. This is true during normal heat pipe operation, when the evaporator surface is illuminated by the solar flux, or during operation from storage, when evaporation occurs on the surface of the integral storage capsules.

The temperature profile shown in the figure on the underside of the inlet plenum was calculated from an energy balance. Heat input to the surface is the result of illumination from the concentrator and reradiation from the heat pipe evaporators. The heat is rejected to the gas by convection and by radiation to the aperture and to other surfaces in the inlet plenum assembly. These temper-

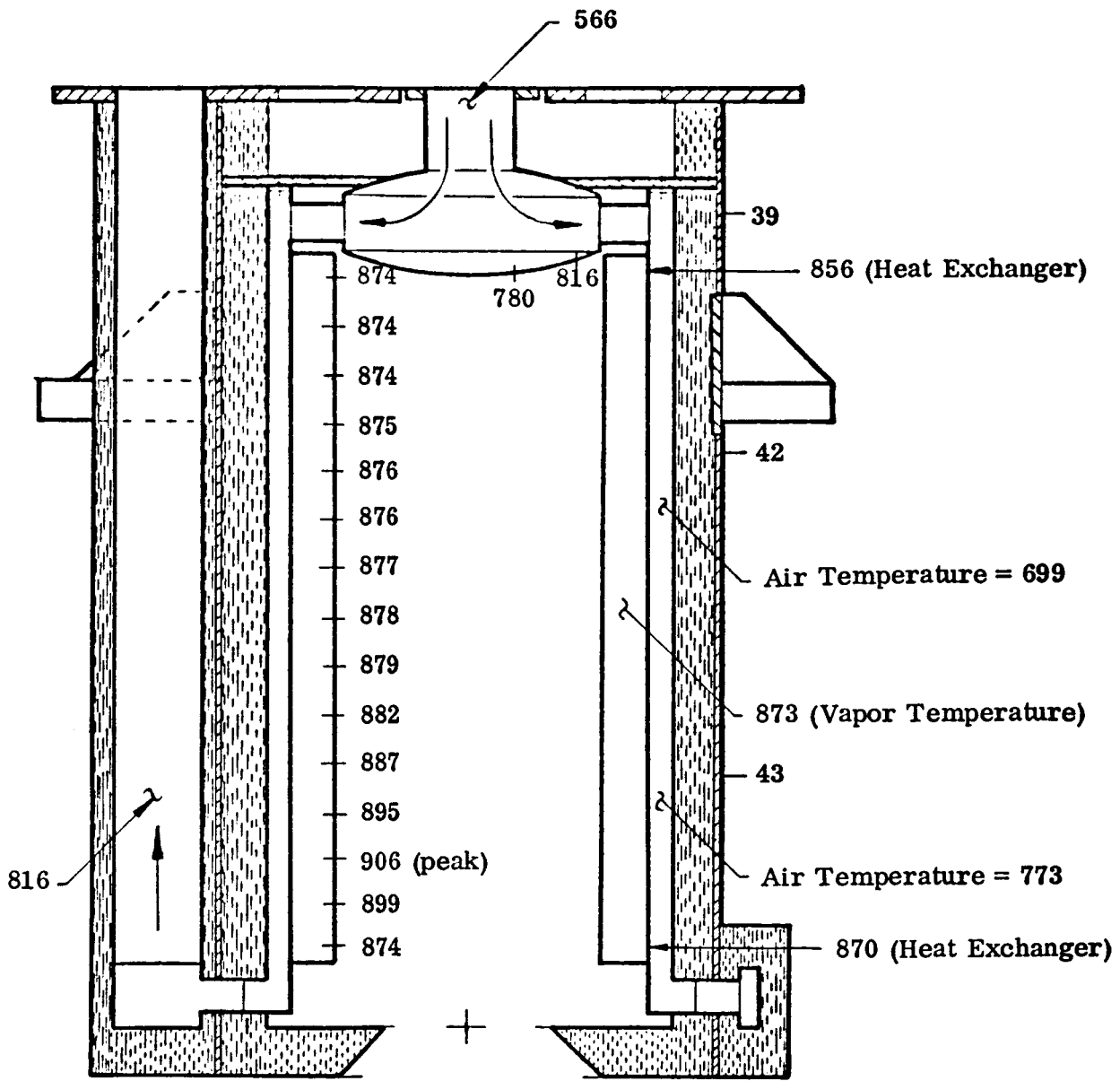

FIGURE 4.2

RECEIVER TEMPERATURE AT DESIGN POINT (^{o}C)

atures pose no significant design problem for the plenum provided it is made from stainless steel. If low alloy steel is used instead, a protective insulation will be used to shield the surface.

The efficiency of the baseline receiver at the design point was evaluated parametrically as a function of wind speed and insulation thickness and conductivity. Thermal losses considered in the evaluation included conduction losses through insulation surrounding the exit duct, the toroidal exit plenum, and the bulk of the receiver, and radiation and convection losses from the aperture. The convection losses from the aperture were treated in considerable detail, using an equation utilized by Honeywell[1] for a similar cavity receiver. This convection loss becomes an appreciable portion of the total losses. The receiver is insulated with an alumina-silica fiber, which is either in blanket or rigidized form, and with a borosilicate glass fiber blanket. The alumina-silica insulation is a high temperature insulation, usable at temperatures up to 1320°C. In blanket form, it is used around the exit plenum and duct, inside the cylindrical receiver casing, and at the top of the receiver. A rigidized form of the same insulation is used at the bottom of the receiver. The borosilicate glass fiber blanket can only be used at temperatures up to 400°C. It is used outside the cylindrical receiver casing. The insulation of the receiver is discussed in more detail in Section 5.

The efficiency of the receiver is shown in Figure 4.3 as a function of wind speed. The efficiency is referenced to a design power input of 68.6 kW. Below the figure, the distribution of losses are shown at a wind speed of 16.1 km/hr (10 mph). From this distribution, it is obvious that the receiver is insulated quite effectively, as only 25% of the losses are due to convection from insulated surfaces. The remainder of the losses occur through the aperture, with convection losses accounting for 43% of the total, and radiation accounting for 32%. The importance of the convection losses from the aperture indicated by this breakdown is unfortunate, in that this loss is the most difficult to determine. Very few empirical relationships exist which define convective losses from cavities. If convection losses are indeed

(1) Solar Pilot Plant, Phase 1, Preliminary Design Report, Volume 2, Honeywell Inc., May 1, 1977

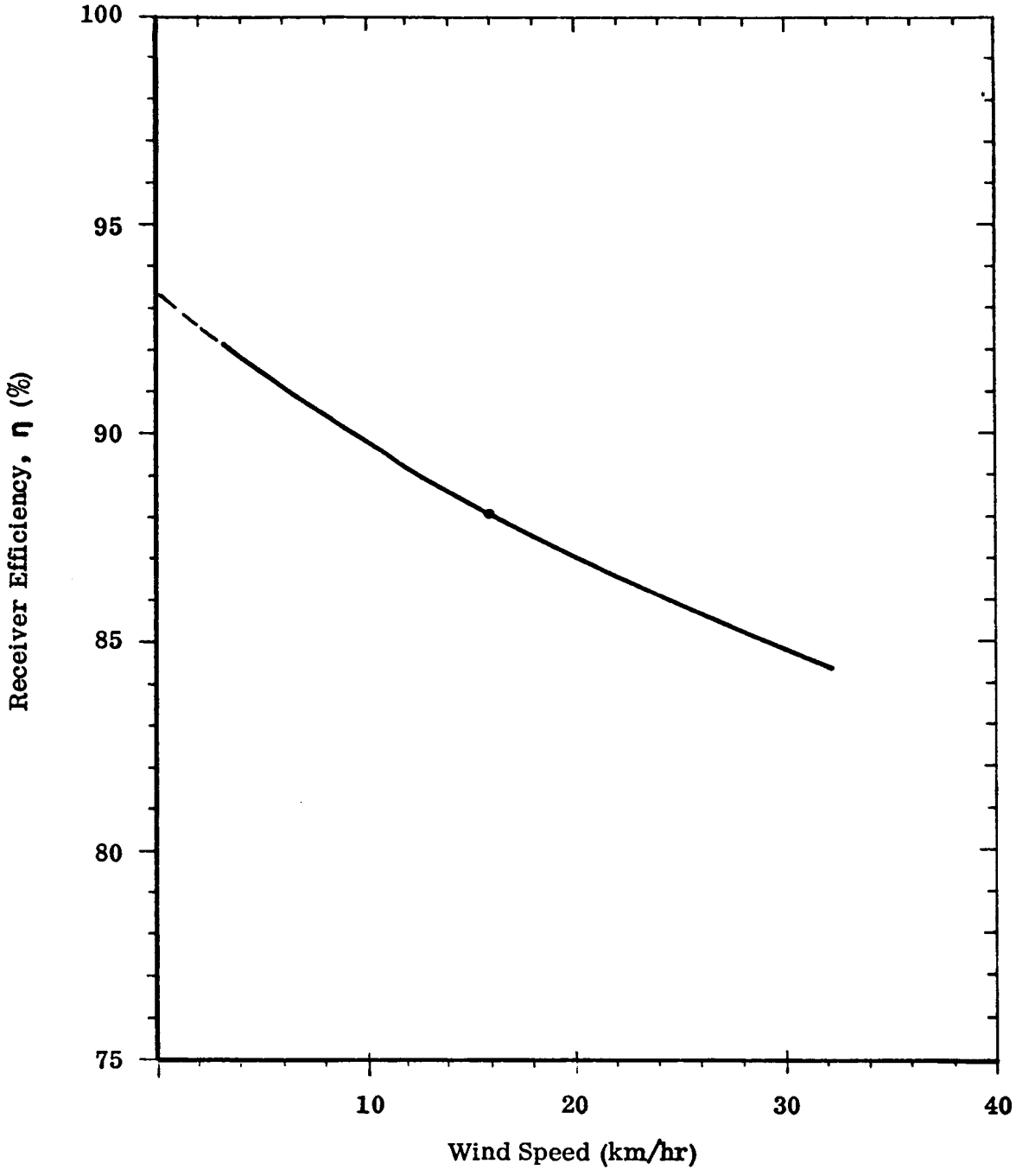

Distribution of Losses for Wind Speed = 16.1 km/hr*

Radiation from Aperture	3.66%
Convection from Aperture	5.07%
Exhaust Duct	0.28%
Toroidal Exhaust Planum	1.53%
Bulk of Receiver	1.13%
Total	11.67%

*Losses are referenced to design thermal input of 68.6 kW

FIGURE 4.3 RECEIVER THERMAL EFFICIENCY

this high, efforts to suppress convection at the aperture is certainly worthwhile.

The performance of the receiver was also characterized in terms of pressure losses through the receiver. This evaluation includes the pressure drop through the inlet duct and plenum, through the heat pipe manifolds and heat exchanger, and through the exit plenum and duct. Pressure losses due to friction and momentum through the various expansions, contractions, and turns in the air flow path are included. Figure 4.4 shows the distribution of losses throughout the receiver. The total pressure drop, which is based on a design air flow rate of 0.24 kg/sec, is 2.57 KPa (0.37 psi). The largest single component of the total loss occurs through the air heat exchanger (38%). Of the remaining pressure loss, 26% of the total occurs prior to the heat exchanger and 34% occurs downstream of the heat exchanger.

One assumption which is inherent in this analysis is that the air flow rate through each heat pipe is identical. To accomplish this, the cross sectional area of the exit plenum has been varied around the circumference of the receiver. Up to this point in the air path, the flow resistances are the same. The size variation within the exit plenum maintains the pressure loss, due to expansion into the torus and circumferential flow around the torus, identical for all heat pipes. As a result, the flow resistance associated with all heat pipes are equalized and no additional controls are required to maintain an air flow balance.

The discussion of receiver performance thus far has been based on a design point thermal input of 68.6 kW, which is consistent with the specified temperature rise of the air through the receiver and the design air flow rate. Receiver performance was also evaluated at a peak power input of 85 kW. At this thermal input, it was assumed that the mass flow rate was increased by 24% to maintain the same temperature rise in the air. The crucial performance parameters of the receiver at peak and design power are compared in Table 4.2. The temperature's distribution within the receiver changes very little between the design and peak power. The heat pipe vapor temperature increased by 11^{o}C and the maximum cavity temperature increases by 18^{o}C. The increase in maximum temperature exceeds the vapor temperature increase because the incident fluxes and

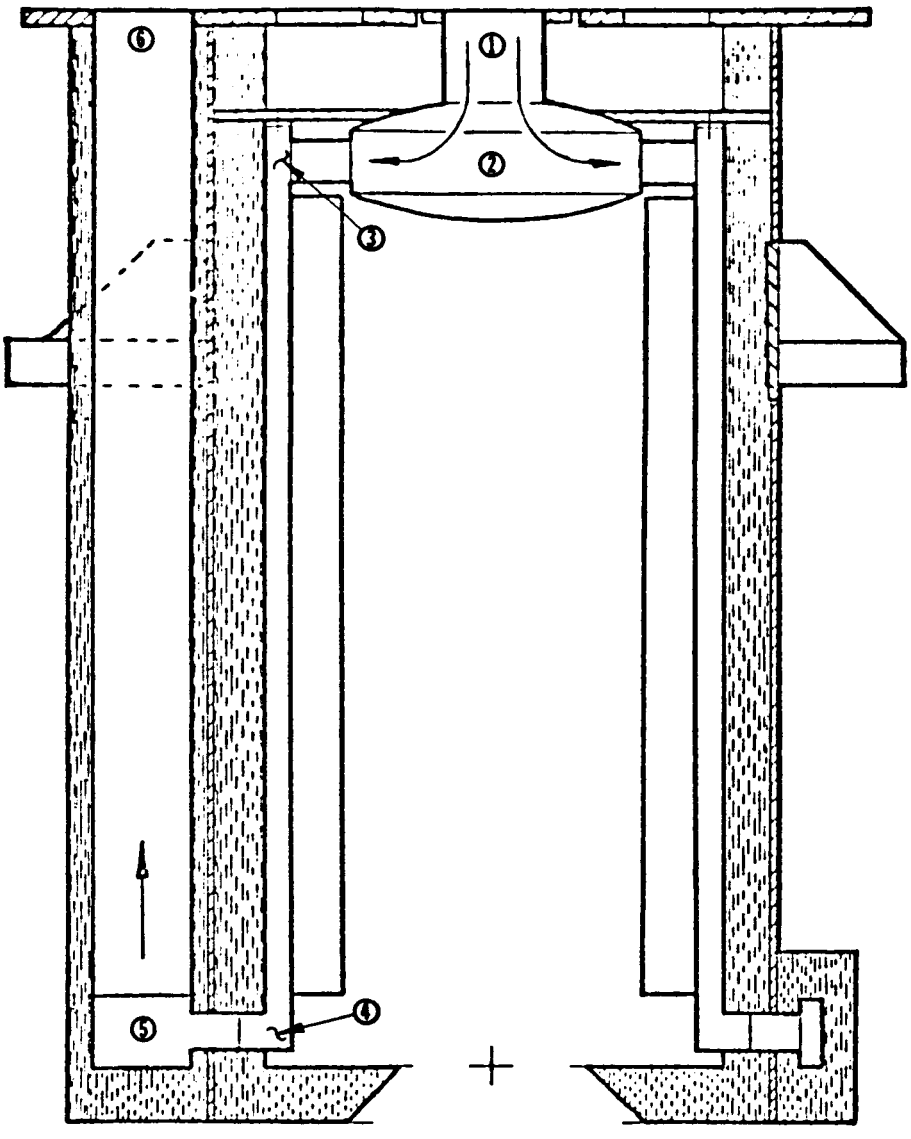

Location	ΔP (KPa)/(psi)
Inlet Duct (1)-(2)	.485/.070
Inlet Manifold (2)-(3)	.204/.030
Heat Exchanger (3)-(4)	.987/.143
Exit Manifold (4)-(5)	.446/.064
Exit Duct (5)-(6)	.446/.065
Total (1)-(6)	2.57/0.372

FIGURE 4.4

PRESSURE LOSSES IN THE RECEIVER

PARAMETER	Peak Power	Design Point
Thermal Input (kW)	85	68.6
Air Inlet Temperature (^{o}C)	566	566
Air Outlet Temperature (^{o}C)	816	816
Air Mass Flow Rate (kg/sec)	0.30	0.24
Receiver Efficiency (%)*	90.3	88.3
Receiver Pressure Drop (kPa)	3.93	2.57
Heat Pipe Vapor Temperature (^{o}C)	884	873
Maximum Cavity Temperature (^{o}C)	924	906

*At Wind Speed of 16.1 km/hr

TABLE 4.2

RECEIVER PERFORMANCE SUMMARY
AT PEAK AND DESIGN POWER

therefore the gradient through the wall were assumed to increase at the same rate as the total input power. The receiver efficiency at peak power is slightly higher than at design power. The reason for this is that at higher powers the receiver temperatures and hence the heat losses increase at a slower rate than the input power. The greatest difference in performance between peak and design power occurs in the receiver pressure drop. This pressure drop increases with the square of air flow rate

4.2 Receiver Performance at Off-Design Conditions

Receiver behavior was also analyzed at off-design conditions. As one part of this evaluation, the diurnal behavior of the receiver with typical daily variations in insulation conditions was investigated. Two different turbine control techniques were considered, consisting of constant turbine speed and constant turbine inlet temperature. These two control schemes are represented schematically in Figure 4.5. For the use of constant turbine inlet temperature, the turbine is not activated until the receiver temperature reaches the design point of 816^{o}C. Then the turbine is started and its speed adjusted to maintain the turbine inlet temperature at the design point. This requires the speed be adjusted in accordance with the level of solar insolation. Turbine speed is than maintained constant until the insolation begins to decrease in the afternoon. The speed is then continually decreased to maintain constant inlet temperature until the losses from the receiver exceed the thermal input, at which point the turbine speed is zero.

For the case of constant turbine speed, the turbine is not activated until the receiver temperature reaches the point where the turbine work is sufficient to drive the compressor (~390^{o}C). At this point, the turbine is brought up to full speed. The turbine inlet temperature continues to rise in accordance with the solar input until the design point is reached. The turbine speed is maintained at the design point until the turbine inlet temperature decreases and reaches 375^{o}C in the afternoon. When this occurs, the turbine is turned off.

Figures 4.6 and 4.7 show the predicted diurnal performance of the baseline receiver design with constant turbine inlet temperature and with constant turbine

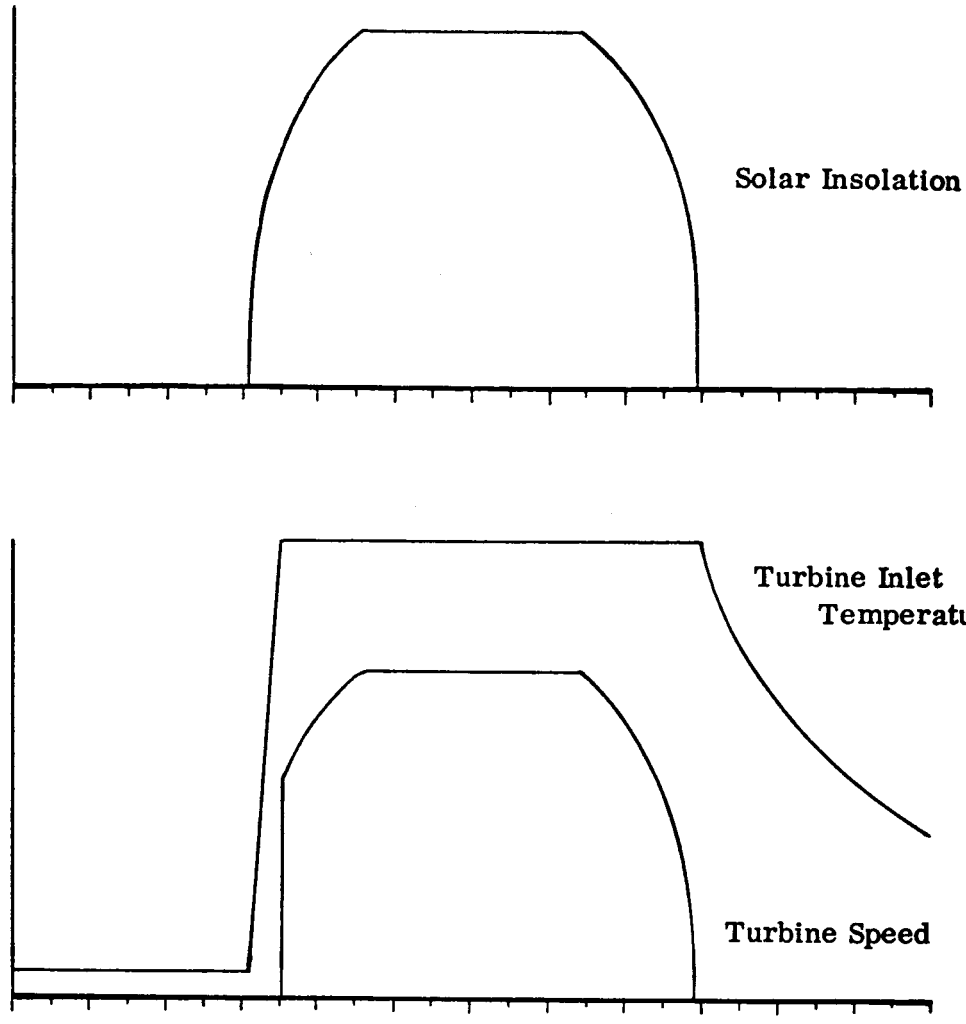

A. Constant Turbine Inlet Temperature

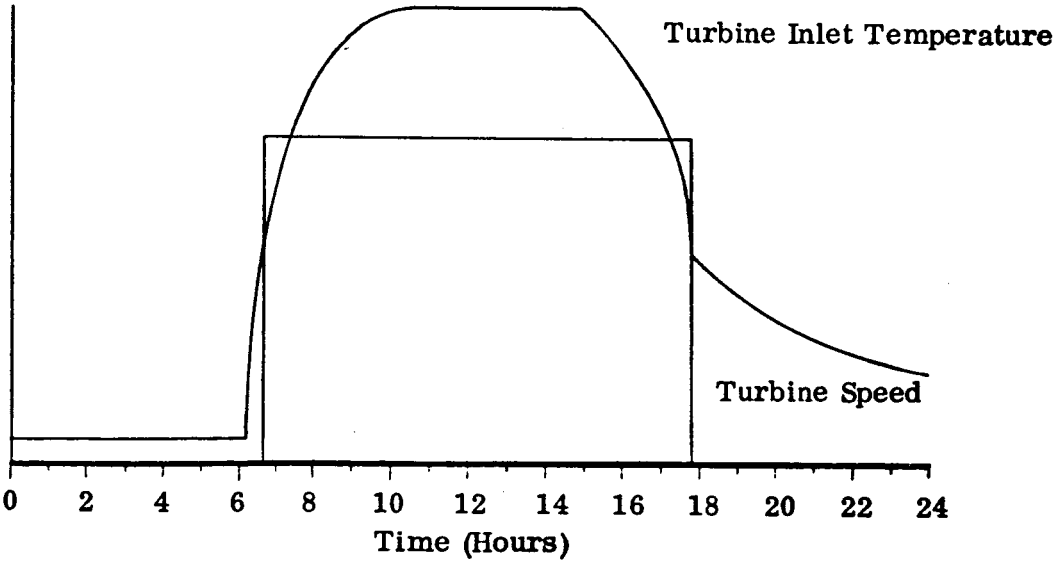

B. Constant Turbine Speed

FIGURE 4.5. TYPICAL DIURNAL CONTROL SEQUENCES

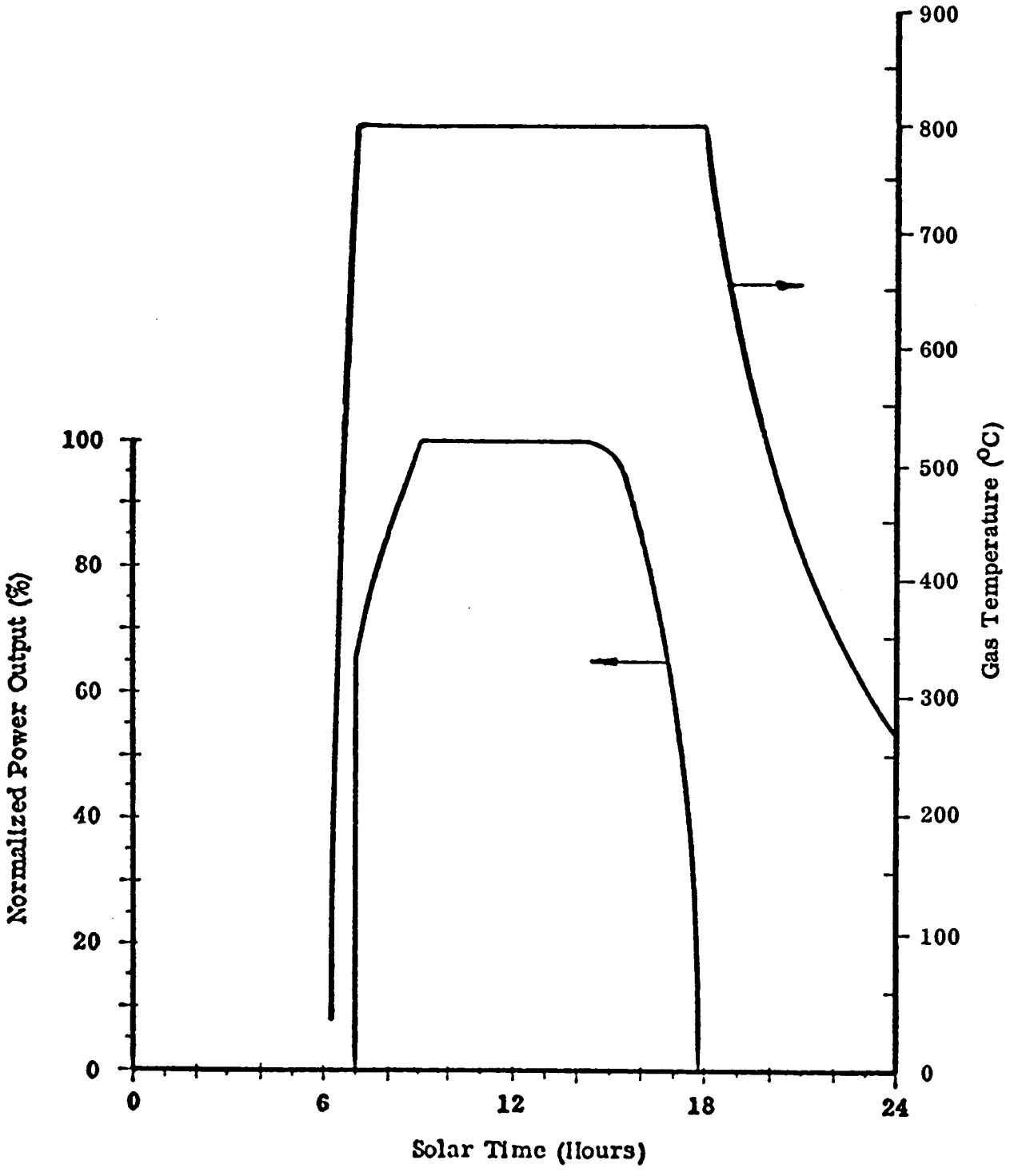

FIGURE 4.6

DIURNAL RECEIVER PERFORMANCE
(CONSTANT TURBINE INLET TEMPERATURE)

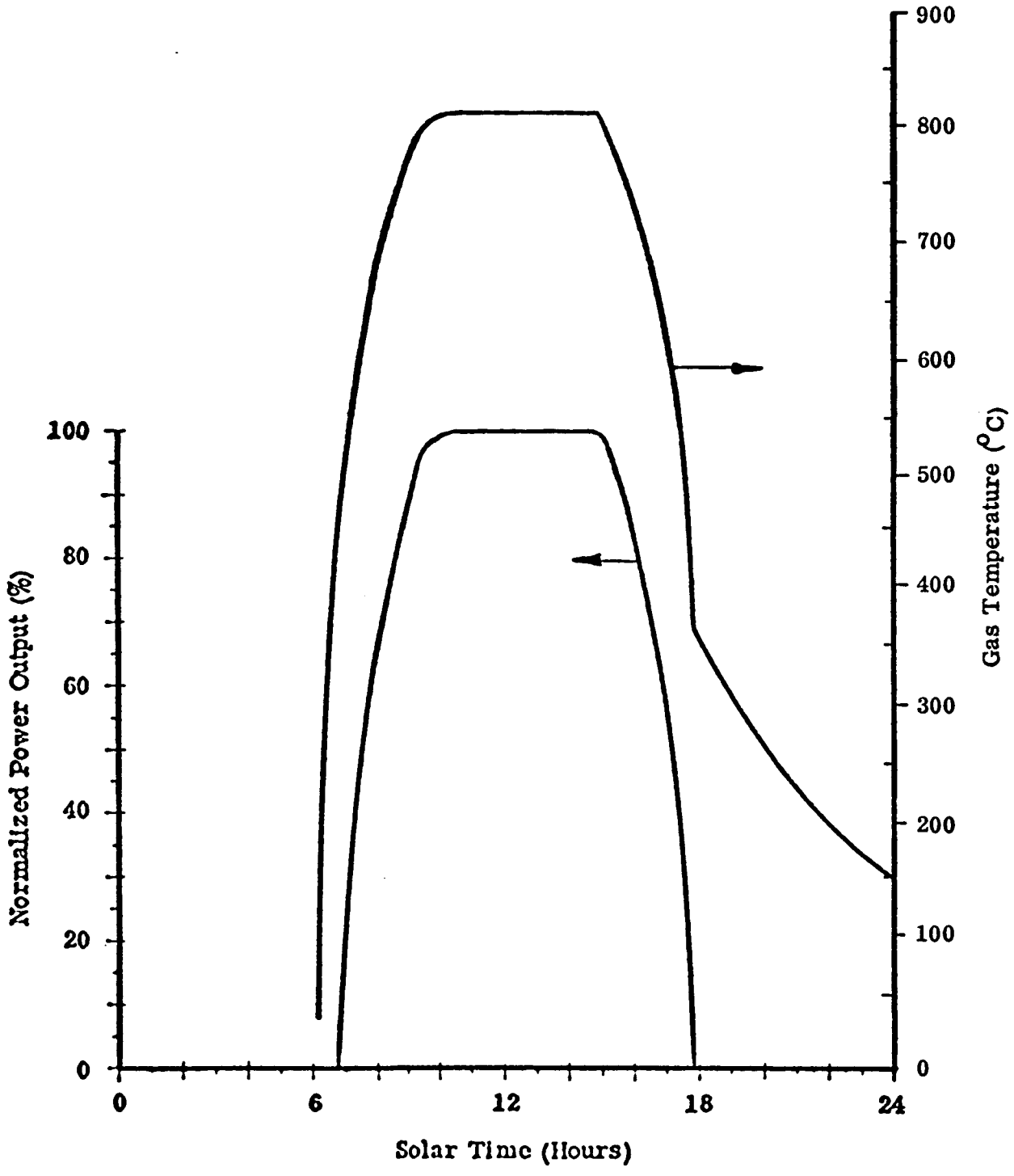

FIGURE 4.7

DIURNAL RECEIVER PERFORMANCE
(CONSTANT TURBINE SPEED)

speed, respectively. In each figure, the receiver temperature and the normalized power output of the cycle is shown over the course of a typical day. Integration of the power output curves from both figures indicates that the total energy provided with constant inlet temperature control is 6% greater than the energy provided with constant turbine speed control. It is obvious from the figures that the receiver was assumed to be initially at ambient temperature. However, in both cases, the receiver temperature does not decrease to ambient by the following sunrise. But the rate of rise of the receiver temperature in the morning is quite rapid and hence the results will not change significantly.

Receiver behavior was also characterized for solar insolation considerably below the peak solar input. At reduced insolation levels, maintaining constant turbine inlet temperature is more attractive than maintaining constant turbine speed. In the former case, the thermal input and the output power remain roughly proportional to their design values; while in the latter case, the output power decreases more rapidly than the thermal input. Consequently, it was assumed that turbine inlet temperature was maintained at the design point. It was also assumed that the air mass flow rate is proportional to the input power and that the flux distribution within the cavity remains spatially the same and that its magnitude is also proportional to the input power. For these assumptions, the steady-state performance of the baseline design was evaluated at thermal inputs of 25% and 50% of the peak values. The important characteristics of the receiver's behavior at these reduced inputs are compared to design point values in Table 4.3. The heat pipe vapor temperature exhibits a peculiar trend, first increasing and then decreasing as the input power drops. This is due to the changes experienced by the film coefficients within the heat exchanger as the flow becomes laminar. The other trends evidenced in the table are not unexpected. The receiver efficiency at reduced power are lower than the design point since the receiver temperatures and hence thermal losses tend to remain constant while the power is decreased. The pressure drop through the receiver shows marked reductions at reduced power since it is roughly proportional to the square of the mass flow rate.

PARAMETER	Design Point	50% Power	25% Power
Air Flow Rate (kg/hr)	872	436	218
Heat Pipe Vapor Temp. (^{o}C)	873	909	839
Maximum Cavity Temp. (^{o}C)	906	926	847
Receiver Efficiency (%)*	88.2	75.1	55.6
Receiver Pressure Drop (kPa)	1.94	.50	.19

*At Wind Speed of 16.1 km/hr

TABLE 4.3

RECEIVER BEHAVIOR AT REDUCED THERMAL INPUT

4.3 Receiver Operation with Buffer Storage

The analysis discussed thus far has been practically independent of the buffer storage system. The steady-state performance of the receiver and long-term diurnal transients are not influenced appreciably by the thermal mass of the buffer storage system. However, a considerable amount of program effort was devoted to the evaluation of receiver operation from storage during short-term transients such as those resulting from intermittent cloud cover. Several candidate storage systems were examined and compared on the basis of output power as a function of time. It was assumed that all candidate systems had the same volume and that the selected volume could be easily fitted inside the heat pipe envelope. Each candidate system was evaluated for the same initial condition; that is, the receiver operating at the design point prior to solar outage. It was assumed that the turbine control technique employed during the outage maintains turbine speed constant at the design level.

Receiver performance with two buffer storage systems is shown in Figure 4.8. The figure shows the power output of the cycle as a function of operating time with a eutectic salt ($LiF-MgF_2$) and with iron. Two curves are shown for the salt. One curve represents the behavior of an idealized salt which is assumed to be an isothermal medium. Idealized behavior can be approached by designing the salt storage container to enhance the conductance of the salt. The other curve represents the behavior of the salt at the other extreme; that is, where the conductance of the storage medium is strictly a function of the thermal conductivity of the salt. These two curves fix the upper and lower performance limits for the salts. The third curve shown in the figure represents the performance capabilities of an iron buffer storage system. The iron was also assumed to be an idealized medium; however, since the thermal conductivity of iron is an order of magnitude greater than the salt, the effects of conduction should be minimal.

To analyze the effects of conduction on the salt system behavior, a simplified nodal network was used to model the salt and its container. The salt was divided into three concentric nodes of equal volume. Heat removal from the salt can be characterized into three distinct regions which are also shown in Figure

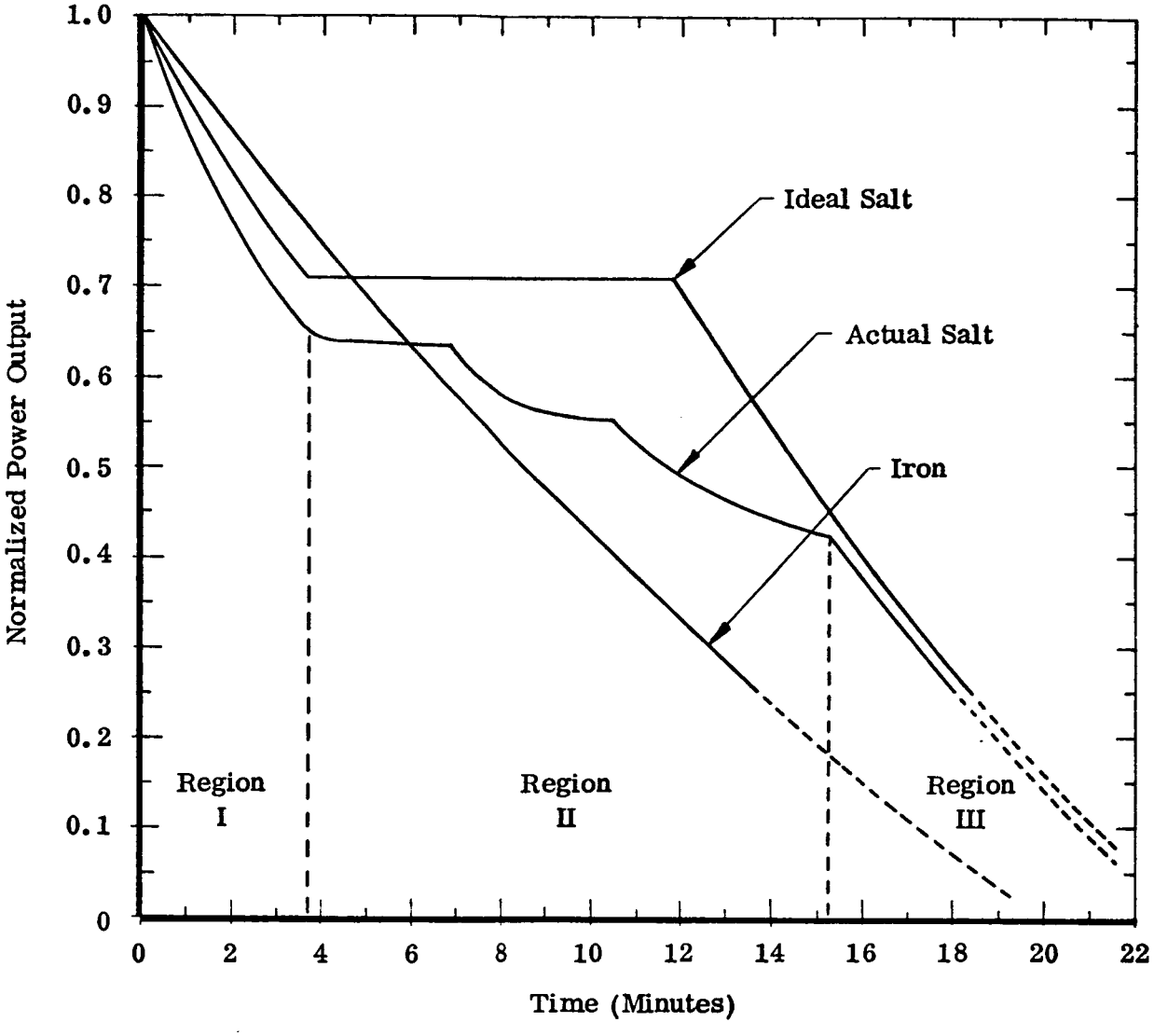

FIGURE 4.8

BRAYTON CYCLE OUTPUT FROM STORAGE

4.8. The first region begins with the salt isothermal at the design vapor temperature and ends when the temperature of the outermost salt node reaches the freezing temperature. In this region, the energy supplied to the cycle is sensible heat from the liquid salt and the containers. In the second region, freezing gradually proceeds radially inward until all the salt is frozen. As the salt in each node freezes, the temperature of the node is maintained at the freezing temperature. The three distinct steps in Region 2 represent the duration of freezing within each salt node. Obviously, if more nodes were used the curve would be much smoother. The third region begins after the salt is frozen and extends until the power output of the cycle falls below usable limits (defined as 25% of design power). In this region, the solid salt yields its sensible heat. Notice that the behavior of the idealized salt can also be characterized according to these three regions. The only difference is that freezing occurs while the entire salt volume is maintained at the freezing temperature.

The relative performance of various buffer storage systems is best evaluated by comparing the operating time and the total power output of the cycle during solar outage. Both parameters were evaluated between the time when solar outage first occurs until the output power falls to 25% of the design output. Table 4.4 presents a summary of these and other critical parameters, such as weight and cost, of four candidate storage systems. In addition to those two systems previously discussed, another sensible heat system, using beryllia and another eutectic salt, $NaF-MgF_2$, were evaluated. All comparisons are based on the assumption of constant volume. The sensible heat systems which were evaluated were selected because of their high heat capacity and also because of their compatibility with sodium. Both salt systems have melting temperatures at the upper end of the heat pipe operating temperature range. $NaF-MgF_2$ melts at 832°C. $LiF-MgF_2$ melts at a lower temperature (741°C) but its latent and sensible heats are considerably higher than the sodium salt.

All of the candidate storage systems summarized in the table are capable of operating for the required 10 minutes. The most attractive storage medium is $LiF-MgF_2$. However, Inconel 617 is required for the salt storage capsule. This

Storage Material	$LiF-MgF_2$ (Ideal)	$LiF-MgF_2$ (Actual)	$NaF-MgF_2$ (Ideal)	Iron	Beryllia
Storage Container	Inconel 617	Inconel 617	Inconel 617	---	---
Weight of Storage Material (Kg)	31.1	31.1	31.6	144	55.4
Total TES Weight	55.8	55.8	56.3	144	55.4
Heat Input from Storage* (kW-hr)	21.6	20.2	16.6	15.7	16.6
Power Output* (kW-hr)	3.40	3.00	2.75	2.30	2.54
Operating Time* (minutes)	18.4	18.1	13.5	13.7	14.5
Unit Cost/Storage Material ($/Kg)	9.01	9.01	8.66	1.94	214
Unit Cost/Storage Container ($/Kg)	12.24	12.24	12.24	---	---
Total Storage System Cost ($) (Storage Material/Container)	585 (280/305)	585 (280/305)	579 (274/305)	282	11,850

*For power output not less than 25% of design power

TABLE 4.4

CANDIDATE STORAGE SYSTEM COMPARISONS (CONSTANT VOLUME)

particular alloy is not commercially available in the small quantities needed for a prototype receiver. Storage capsules for the other salt must also be made from Inconel 617. Of the two sensible heat systems, Beryllia offers the better performance. However, iron, in spite of its poorer performance and higher weight, is more attractive than Beryllia because of its much lower cost. Consequently, iron would be employed as the storage medium in the prototype receiver.

4.4 Receiver Sensitivity to Adverse Operating Conditions

The performance analysis also included the evaluation of the receiver's sensitivity to adverse operating conditions. As part of this effort, the behavior of the receiver with sudden air flow interruption was investigated. It was assumed this interruption occurs at full insolation with the receiver operating at the design point. Figure 4.9 shows the temperature history at that point in the receiver where the temperature is highest. Two curves are presented; one with a $LiF-MgF_2$ storage system and the other with an iron storage system. But curves assume radiation losses from the receiver but neglect convection losses. As it turns out, over the temperature range of interest, the assumed losses have very little effect on the temperature rise.

The survival time of the receiver during air flow interruption is basically determined by the heat pipe assemblies. It was assumed that the receiver is designed to accommodate thermal expansions during over-temperature and that the maximum allowable temperature of the other components, such as the insulation and gas manifolds, are not exceeded. The maximum allowable temperature of the heat pipe assembly could be the result of pressure containment problems of sodium at high temperatures, temperature induced stresses through the heat pipe wall, differential thermal expansion of various parts of the assembly, or degradation of materials of construction at elevated temperatures. Of these considerations, the limiting temperature is determined by pressure containment when stainless steel 310 is used for the heat pipe envelope. For 2-inch IPS Schedule 5 pipe, the maximum allowable temperature is $960^{o}C$. If Inconel 601 is used instead, the maximum temperature is determined by thermal stresses. For the same pipe size, the maximum

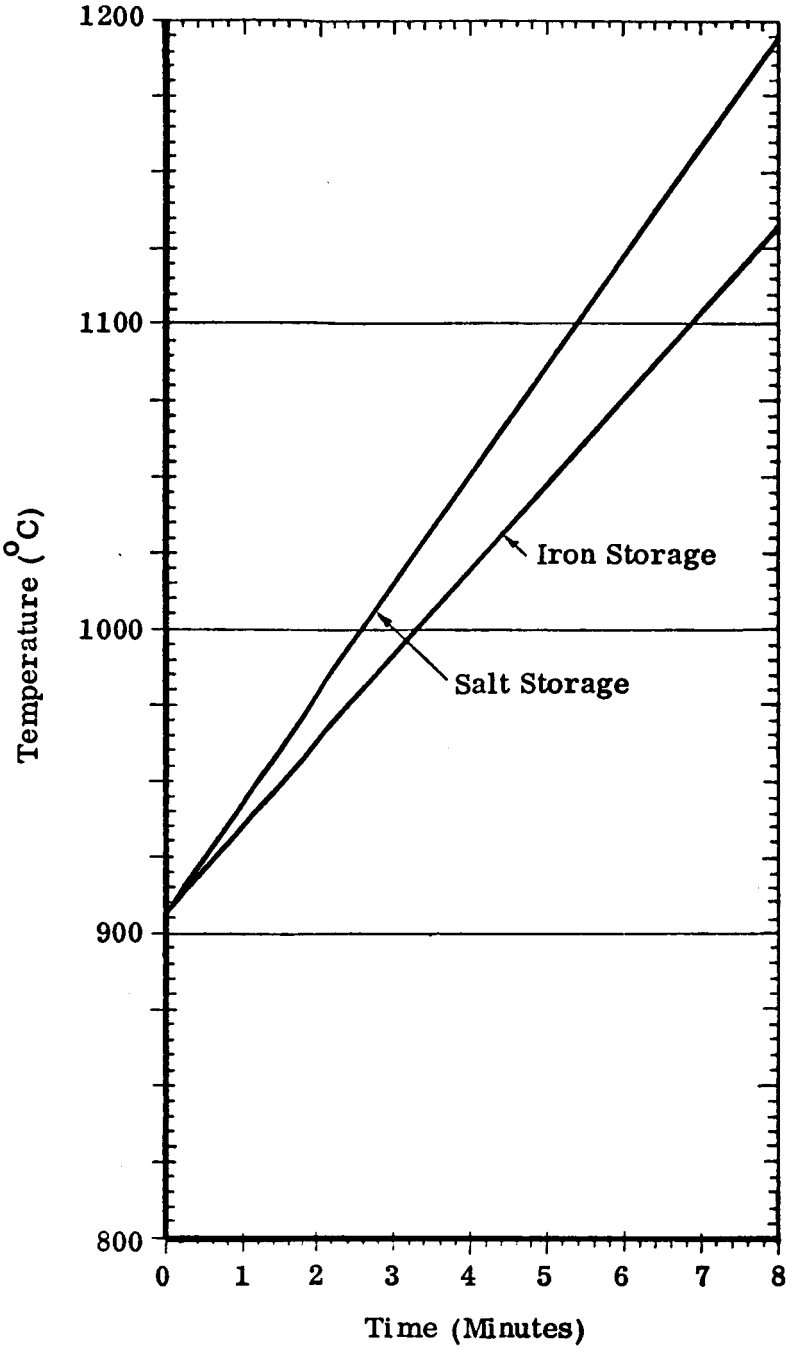

FIGURE 4.9

TEMPERATURE RISE OF THE RECEIVER FOR NO AIR FLOW

temperature becomes 1050°C. Consequently, with stainless steel heat pipes, the survival time from Figure 4.9 is shown to be 1.5 minutes with salt storage and 1.9 minutes with iron storage. With inconel, these times become 4.0 minutes for salt storage and 5.1 minutes with iron.

Receiver sensitivity to misalignment was also investigated. The purpose of this analysis was to determine the maximum allowable distance which the receiver centerline could be displaced radially from the focal point. It was assumed that the radial displacements were not accompanied by angular displacements. The flux profiles used in the analysis consisted of those curves provided by JPL for the aperture plane and the distributions predicted by Dynatherm's computer program within the cavity. The aperture assembly can tolerate radial displacements of 2.3 cm. At larger displacements, the incident flux on the assembly causes its adiabatic temperature to exceed the maximum service temperature, which will probably cause cracking. Should the aperture assembly fail, the next component which will be exposed to increased levels of insulation are the heat pipes. The radial displacement which results in failure of the aperture assembly should present no particular problem for the heat pipes. The heat pipes should be able to tolerate displacements up to 5.5 cm. At larger displacements, temperature induced stresses on the end caps could cause failure.

4.5 Heat Pipe Performance Requirements

The steady-state performance requirements of the heat pipes are summarized in Table 4.5 for the design input of 68.6 kW and for the peak input of 85 kW. The heat transport requirements, in terms of total heat load, axial flux, and radial fluxes are directly proportional to the thermal input to the receiver. The vapor and metal temperatures, on the other hand, are practically independent of the heat loads. The heat pipes are required to operate at practically all orientations from horizontal to vertical, although at low inclinations the loads are considerably lower than those shown in the table. Basically, these loads are applicable only at heat pipe tilts greater than 30 degrees.

These performance requirements present no particular problems for liquid

PARAMETER	Peak Power	Design Power
Heat Load per Heat Pipe (Watts)	4470	3610
Evaporator Flux (MW/m^2)	0.405	0.327
Axial Flux (MW/m^2)	2.17	1.75
Condenser Flux (MW/m^2)	0.234	0.189
Vapor Temperature (^oC)	884	873
Maximum Metal Temperature (^oC)	924	906
Orientation	Horizontal-Vertical	Horizontal-Vertical

TABLE 4.5

HEAT PIPE PERFORMANCE REQUIREMENTS

metal heat pipes. Sodium is well suited for operation at this temperature. Its liquid properties are conducive to high heat transport, and its low vapor pressure does not result in any containment problems. The required axial and radial fluxes have been achieved with sodium heat pipes of the same size in this temperature range.* Another attractive feature of sodium is its compatibility with candidate materials for the heat pipe envelope, notably stainless steel and inconel.

The wide range of heat pipe orientations stipulates that some care be exercised in routing the air through the heat pipe heat exchanger. To facilitate heat pipe operation, it is desirable to promote condensation above evaporation and thereby utilize gravity to aid condensate return to evaporation sites. For this reason, the air enters the receiver at the top and is gradually heated as it flows downward. Condensation occurs at the greatest rate where the air is coldest, and consequently the bulk of the condensation occurs at the uppermost parts of the heat pipe.

The heat pipes must also be capable of operating under the transient conditions associated with the daily operation of the ABSR. At the very least, this will include diurnal startup and shutdown and could also involve startup after solar interruption. The key factors in heat pipe startup are the initial distribution of the liquid and the dynamic of the vapor. With regard to the fluid distribution, two cases must be considered: (1) cool-down of the receiver below the freezing point of sodium (98^{o}C), and (2) startup with liquid sodium in the heat pipes. If the fluid is frozen, the initial distribution will depend on the orientation of the heat pipe during shutdown. The wick structure in these heat pipes is capable of wicking approximately 30 cm. So for stow positions of the receiver within roughly 15 degrees of horizontal, the wick structure will remain saturated during shutdown. If the receiver is stowed vertically (above the concentrator), roughly one-third of the evaporator would remain saturated. Fortunately, that portion of the wick structure which remains saturated is located in the section of the pipe which is subjected to the highest flux during restart. Stowing the receiver vertically, but with the concentrator inverted, would freeze-out the fluid in the wrong section of the heat pipe

*"Liquid Metal Heat Pipes for the Central Solar Receiver," by Walter Bienert and David Wolf, 13th IECEC, Paper No. SAE/P-78/75

and would cause a fluid deficiency in the high flux section of the heat pipe. If this latter stowing mode were to be used, the wick would have to be redesigned and liquid traps incorporated near the bottom of the heat pipes. In the case that the receiver temperature does not fall below the freezing point of sodium during shutdown, no problems are anticipated. The fluid will assume proper distribution as soon as the receiver is oriented for operation.

The other consideration during startup is the vapor dynamics. Its significance will depend on the turbine control technique which is utilized. If constant turbine inlet temperature is the preferred mode of operation, then the air flow would not be started until the receiver reaches the design point temperature. However, if turbine speed is kept constant, the turbine could be activated at inlet temperatures as low as 390°C. At this temperature the thermal input to each heat pipe, as determined by the power conversion cycle, is 1730 Watts and the heat pipe vapor temperature is 420°C. As the turbine speed is maintained and the thermal input to the receiver gradually increases, both the heat pipe vapor temperature and the thermal input to the heat pipe gradually increase to their design values.

During this type of startup, vapor dynamic effects may dominate the performance of the heat pipes. Vapor flow considerations limit the local vapor velocity to no more than sonic velocity and restrict the overall vapor pressure drop to no more than the absolute vapor pressure. A typical vapor limit curve is shown in Figure 4.10 in terms of axial flux versus heat pipe vapor temperature. Also shown in the figure is the required axial heat flux during startup in the constant speed mode of operation. At vapor temperatures below 460°C, the transport requirements exceed the sonic limit. As a result, below 460°C heat pipe performance will coincide with the sonic curve. Since the sonic limit represents a vapor limitation and not a capillary wick limit, attempts to operate above the sonic limit do not result in hydrodynamic failure of the heat pipe. Instead, attempts to operate at powers which exceed the sonic limit result in automatic increases in heat pipe vapor temperature to conform to the sonic curve.

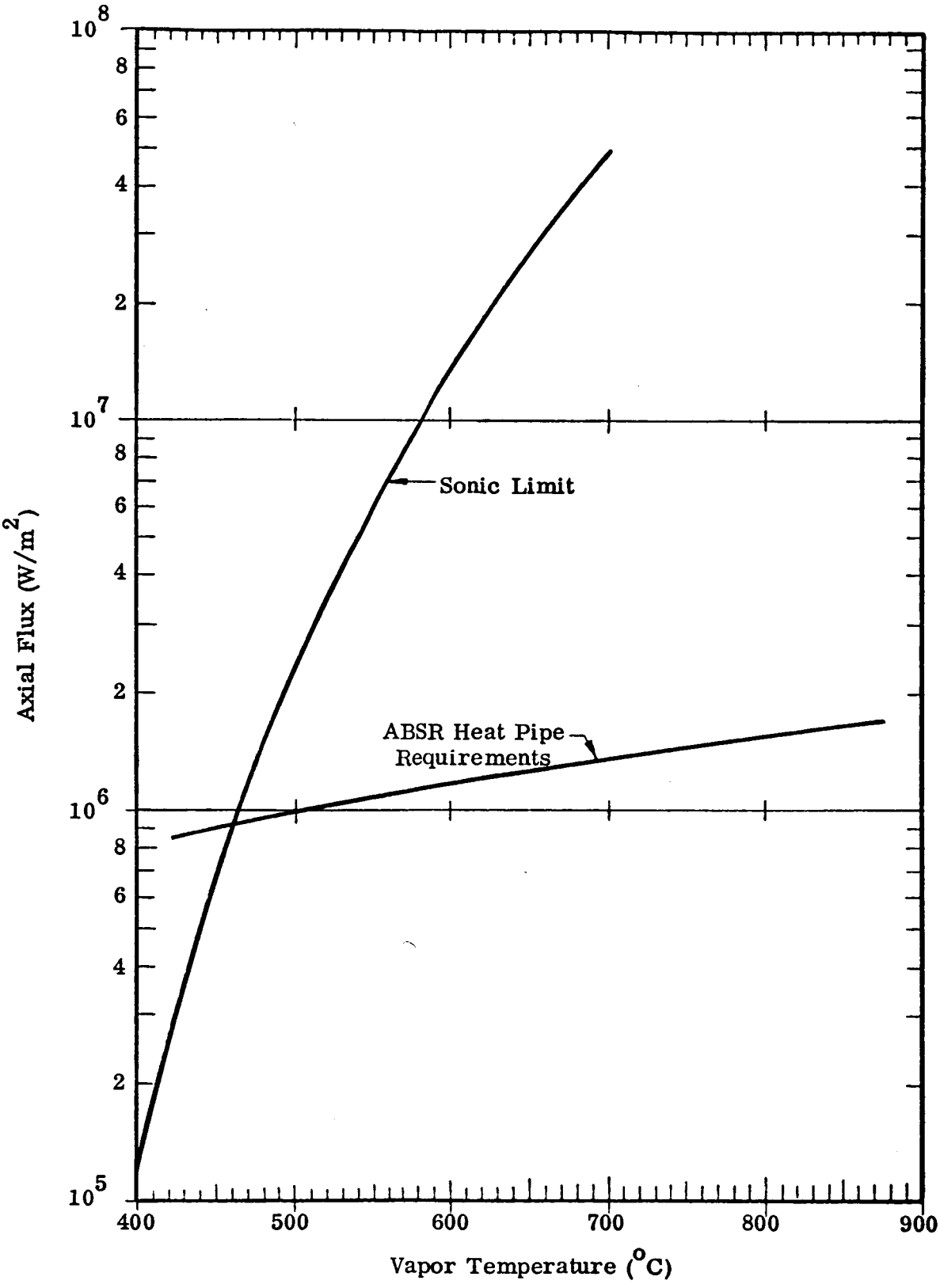

FIGURE 4.10

ABSR HEAT PIPE AXIAL FLUX REQUIREMENTS
(CONSTANT TURBINE SPEED)

5. MECHANICAL DESIGN

The baseline design is shown schematically in Figure 2.1 and in detail in the following drawings:

0155-3000	ABSR Assembly
0155-3001	Receiver - PCU Interface
0155-3002	Heat Pipe-Heat Exchanger Assembly
0155-3003	Heat Pipe Assembly
0155-3004	Storage Capsule Assembly

The ABSR has been divided into seven subsystems with further division of the heat pipe/heat exchanger subsystem into three subassemblies.

1.0 Heat Pipe/Heat Exchanger Subsystem
- 1.1 Storage Capsule
- 1.2 Heat Pipe
- 1.3 Heat Exchanger

2.0 Inlet Duct/Plenum Subsystem

3.0 Exit Duct/Torus Subsystem

4.0 Aperture

5.0 Structure

6.0 Insulation

7.0 Hardware

Table 5.1 presents a detailed list of the parts used in the receiver. The parts are characterized in terms of material, size and configuration, and weight.

This section of the report discusses the mechanical design of each of the subsystems. The fabrication procedure utilized in receiver assembly is also presented. At the end of the section, a brief discussion of the structure analysis of the receiver is included.

Assembly	Part	Material	Configuration	Size	Total Weight (lb)
1.0 Heat Pipe Heat Exchanger					564
1.1 Storage Capsule					370
1.1.1	Storage Mtrl.	Iron	Rod	1.625" dia x 30" long	355
1.1.2	Wick	304 S/S	100 Mesh	---	3
1.1.3	Wick	304 S/S	40 Mesh	---	12
1.2 Heat Pipe					98
1.2.1	Envelope	310 S/S	Tube, End Cap	2.375" dia x 0.065" wall	91
1.2.2	Wick	304 S/S	100 Mesh	---	3
1.2.3	Fill Tube	304 S/S	Tube	0.25" OD x 1"	1
1.2.4	Fluid	Sodium	---	---	3
1.3 Heat Exchanger					95
1.3.1	Fins	310 S/S	Sheet	0.07" thick	54
1.3.2	Shroud	310 S/S	Sheet	0.035" thick	25
1.3.3	Headers	304 S/S	Sheet	0.035" thick	7
1.3.4	In/Out Tubes	304 S/S	Tube	1.66" x 0.065"	9
2.0 Inlet Duct/Plenum					46
2.1	Flange	1 Cr $\frac{1}{2}$ Mo St	Flange	$3\frac{1}{2}$ IPS Sch 5	12
2.2	Duct	1 Cr $\frac{1}{2}$ Mo St	Tube	$3\frac{1}{2}$ IPS Sch 5	1
2.3	Plate	1 Cr $\frac{1}{2}$ Mo St	Plate	0.5" thick	19
2.4	Cap	1 Cr $\frac{1}{2}$ Mo St	Cap	12 IPS Sch 5	14

TABLE 5.1

PARTS LIST FOR ABSR

Assembly	Part	Material	Configuration	Size	Total Weight (lb)
3.0 Exit Duct/Torus					114
3.1	Torus	304 S/S	Tube	3½" IPS Sch 5	91
3.2	Locating Pins	304 S/S	Rod	0.5" dia	1
3.3	Exit Duct	304 S/S	Tube	3½" IPS Sch 5	10
3.4	Flange	304 S/S	Flange	3½" IPS Sch 5	12
4.0 Aperture Assem.					17
4.1	Aperture	Cera Form	Board	2" thick	13
4.2	Aperture Support Ring	304 S/S	Sheet	0.032" thick	4
5.0 Structure					291
5.1	PCU Support Plate	HRS	Plate	0.5" thick	93
5.2	Casing	CRS	Sheet	0.040" thick	35
5.3	Upper Support Ring	HRS	Plate	0.25" thick	12
5.4	Inner Rein. Ring	HRS	Tube	0.25" thick	31
5.5	Rec. Mounting Flange	HRS	Plate	0.625" thick	89
5.6	Gussets	HRS	Plate	0.250" thick	14
5.7	Torus Support Ring	304 S/S	Sheet	0.125" thick	17
6.0 Insulation	Blankets	Cerafelt & Microlite			45
7.0 Hardware	Miscellaneous	Misc.			15
Total Receiver					1092

TABLE 5.1

PARTS LIST FOR ABSR (Cont'd)

5.1 Heat Pipe Assembly

The heat pipe assembly consists of three major components: the heat pipe proper, the air heat exchanger, and the buffer storage system. The assembly is shown schematically in Figure 2.2. Nineteen heat pipe assemblies are used in the receiver. They are arranged in a cylindrical pattern around the centroidal axis of the receiver, as illustrated in Figure 2.1. The assemblies are individually manifolded at their upper end to the inlet plenum and at their lower end to the toroidal exit plenum. Each assembly weighs 8.1 kg. Approximately 43% of this weight is associated with the fusible salt buffer storage system.

For the prototype, pure iron is used as the buffer storage medium. This increases the weight of each heat pipe assembly to 13.5 kg, two-thirds of which is associated with the buffer storage. The iron is rod-shaped and placed inside each heat pipe vapor chamber. Comparing the two candidate systems on an equal volume basis, the salt offers better performance. However, it must be encapsulated with Inconel 617. This alloy is difficult to obtain in tubular form in small quantities. In addition, salt storage systems require more development effort than iron systems to establish satisfactory fabrication procedures and compatibility of container materials.

The heat pipe envelope is made from 2-inch IPS Schedule 5, 310 stainless steel pipe. The heat pipe end caps are made from the same alloy. This particular stainless alloy offers relatively good strength and oxidation resistance at elevated temperatures. Thin-walled pipe is used to minimize pseudo stresses due to the wall temperature gradients associated with high incident fluxes. These thermal stresses are considerably higher than the resultant stresses due to structural loads and pressure containment. The stress analysis for the heat pipe assembly is discussed in more detail at the end of this section.

A top view of the completed heat pipe assembly is shown as Section A-A in Figure 2.2. The storage capsule (or the iron rod) is maintained concentric with the heat pipe with standoffs (not shown) welded to its cylindrical surface. The outer surface of the capsule and the inner surface of the heat pipe envelope are lined with circumferential wicks. The wicks consist of one layer of 100-mesh 304 stainless steel

screen which is resistance spot welded to the surfaces. Bridges made from 40-mesh stainless steel screen establish a liquid flow path between the circumferential wicks along the entire length of the pipe.

The same figure also shows a cross section of the air heat exchanger. The heat exchanger extends along the entire length of the heat pipe and is formed by welding five "U" shaped channels along one side of the pipe. The channels are spaced such that the spaces in between channels have the same area as the channels. The channels are enclosed by a shroud, forming a total of nine air passages. The channels and the shroud are made from 310 stainless steel to eliminate stresses which could result from differential thermal expansion of the heat pipe and the heat exchanger. The heat exchanger assembly is completed by welding a manifold and header assembly, made from 304 stainless steel, to both ends. A stud is welded to the upper header to allow heat pipe attachment to the receiver structure.

5.2 Inlet Plenum and Duct Assembly

The inlet plenum and duct assembly consist of the entrance air duct to the receiver, a flange for interfacing with the recuperator exhaust duct, and the inlet plenum. The total weight of the assembly is 21.2 kg. The air temperature throughout the assembly is 566^{o}C; consequently, all components are made from 1% chromium, $\frac{1}{2}$% molybdenum low alloy steel. The inlet duct is made from $3\frac{1}{2}$ inch IPS Schedule 5 pipe. A 150 pound slip-on flange is welded to the top of the duct for interfacing purposes. The inlet plenum is made from a standard 12-inch IPS Schedule 5 cap which is covered by a circular plate. Nineteen holes are drilled in the cap to accommodate the inlet headers of the heat pipes.

5.3 Exit Plenum and Duct Assembly

The exit plenum and duct assembly consist of a toroidal exit plenum, an exit air duct, and a mating flange at the turbine inlet duct interface. The total weight of the assembly is 51.9 kg, 80% of which is in the torus. The air temperature under design conditions throughout the plenum and duct is 816^{o}C. All materials used in the assembly are 304 stainless steel. The exit duct is made from $3\frac{1}{2}$ inch IPS Schedule 5

pipe. At the upper end of the duct, a 150 pound slip-on flange is welded.

The torus is fabricated from four sheet metal walls. The upper and lower surfaces are ring-shaped discs burned from 0.95 cm sheet; and the inner and outer surfaces are made from 0.64 cm sheet, which is rolled and welded into cylindrical shapes. Nineteen holes are drilled on the inner torus wall to allow for heat pipe manifolding. Nineteen locating pins protrude through the lower torus surface. These pins mate with a torus support ring to provide for torus support perpendicular to the receiver's axis, but they permit axial expansion of the heat pipes. The cross-sectional area of the torus varies around the circumference of the receiver; the maximum occurring at the exit duct and the minimum on the opposite side of the receiver. This variation equalized the pressure drop through individual heat pipes and eliminates the requirement for additional controls to maintain an air flow balance through the receiver.

5.4 Aperture Assembly

The aperture assembly consists of two major components: a ceramic disc and a stainless steel support ring. The disc is made from Cera Form Board* which is a rigidized alumina-silica ceramic. The ceramic is lightweight ($\rho = 0.22$ g/cm^3), machinable, and offers good insulating properties which are shown in Figure 5.1. It also has excellent resistance to thermal shock and is suitable for continuous use up to 1430^{o}C. The aperture opening is machined in the center of the disc. In the focal plane, the diameter of the opening is 20.3 cm. This opening intercepts 99% of the energy reflected from the concentrator. The diameter of the opening at the lower edge of the disc is increased to 30.5 cm to avoid additional shadowing of the receiver surface.

The outer edge of the ceramic disc is extended below the torus to provide insulation for its lower surface. Nineteen bolt holes are drilled through the ceramic to allow the aperture support ring, which is made from 304 stainless steel, to be fastened to the receiver structure.

*Tradename of Johns-Manville Product

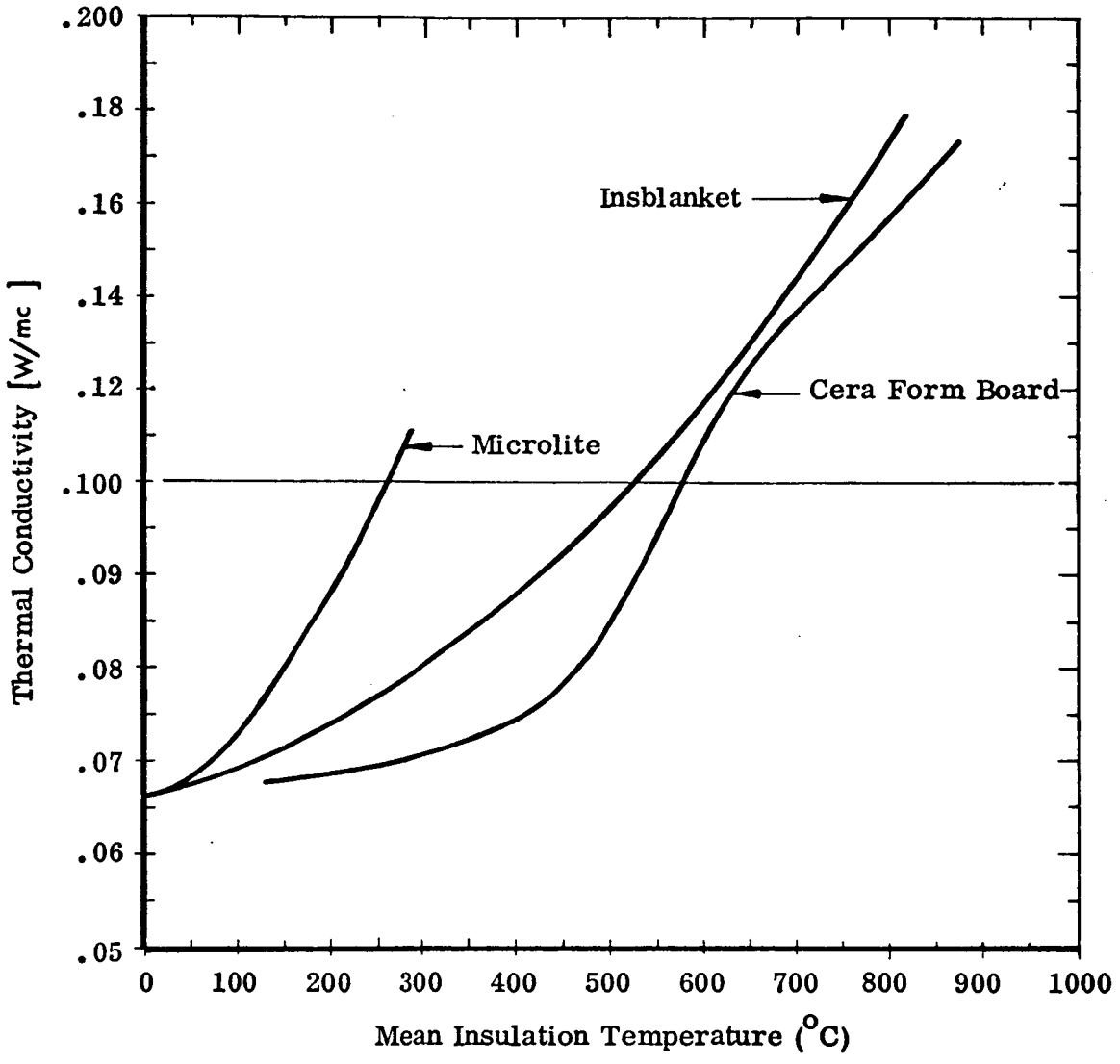

FIGURE 5.1

THERMAL CONDUCTIVITY OF THE
THREE INSULATION MATERIALS USED IN THE ABSR DESIGN

5.5 Receiver Structure

Major components of the receiver structure consist of the receiver-PCU interface plate, the cylindrical casing, a heat pipe support ring, the receiver support ring and gussets, a gusset reinforcement ring, and a torus support ring. All parts of the receiver are made from either hot or cold rolled steel, with the exception of the torus support ring which is 304 stainless steel. The total weight of the receiver structure is 132 kg. The heaviest components are the interface plate, which accounts for 32% of the total, and the receiver support ring, which accounts for another 30% of the total.

The interface plate located at the top of the receiver provides a base to which the PCU is mounted. A plan view of this plate is provided in Drawing DTM 0155-3001. Two holes are provided in the plate to allow for the passage of the inlet and outlet air ducts. These holes are made slightly larger than the duct flanges to facilitate receiver assembly. In addition, several lightening holes will be included. For the weight calculation, it was assumed that 10% of the plate's weight can be eliminated with the holes. These holes are not shown on the drawing since their location will depend on mounting locations for the PCU.

The cylindrical casing is the major structural member in the receiver. It is responsible for transmitting structural loads from the PCU interface plate to the receiver support ring as well as providing support for the other receiver subsystems. The heat pipes are employed as secondary structural members. The inlet plenum and duct is supported in both axial and radial direction by the inlet header assemblies of the heat pipes. The heat pipes also restrain any axial movement of the exit plenum and duct assembly (except for thermal expansion). These structural loads are transmitted from the heat pipes to the casing at the heat pipe support ring which is welded to the casing at a distance 6.4 cm below the interface plate. The casing provides for the cylindrical support of the exit plenum. This is accomplished with a torus support ring which is bolted to the bottom edge of the casing. A bolt hole pattern is drilled into this ring which matches the pattern of the locating pins which protrude from the lower surface of the torus. These holes are elongated in a radial direction to allow for circumferential expansion of the torus relative to the cold receiver structure.

The receiver support ring provides the interface at which the structural loads due to the receiver and the PCU are transmitted to the ultimate support system at the base of the concentrator. Twelve bolt holes evenly spaced around the ring at a radius of 45.7 cm are provided for this purpose. Loads are transmitted from the receiver casing to the support ring via twelve gussets. These gussets are welded to both the support ring and to the casing. In the region where the gussets and the receiver structure meet, a reinforcement ring is welded to the inside of the receiver casing.

5.6 Insulation

The insulated receiver structure is shown schematically in Figure 2.1. Although no distinction is made in this figure, three different kinds of insulation are used. As mentioned earlier, the aperture assembly is made from Cera Form Board.* This rigidized ceramic disc is of sufficient thickness (5 cm) to effectively insulate the bottom of the receiver as well as the underside of the torus. The remainder of the receiver is insulated with Insblanket,** which is a flexible alumina-silica fiber blanket, and Microlite,* which is a flexible borosilicate glass fiber blanket. Insblanket has a density of 0.13 g/cm^3 and its maximum service temperature is 1320°C. Microlite is considerably cheaper than Insblanket and it is also lighter (ρ = 0.016 g/cm^3), but its maximum service temperature is only 400°C. The insulative properties of all three insulations are summarized in Figure 5.1 as a function of bulk insulation temperature.

Insblanket is used to insulate those portions of the receiver inside the receiver shell and the exit plenum and duct. At the top of the receiver, the insulation thickness is 5.0 cm. The space between the heat pipe heat exchangers and the receiver casing, which is 5.0 cm. is also filled with Insblanket. The insulation thickness at the top of the torus is 5.0 cm. Surrounding the exhaust duct and the remainder of the torus is a 7.6 cm thickness of insulation. Outside the receiver casing, a 10 cm thick layer of Microlite extends from the interface plate to the insulation on top of the torus. With this insulation added to the outside of the casing, the temperature of the casing will reach 540°C. The design margin for the receiver structure will allow operation at

*Tradename of Johns-Manville Product
**Tradename of A. P. Green Product

this temperature; however, it is more practical to consider design modifications which will maintain a cooler receiver structure.

5.7 Hardware

In addition to the receiver insulation and those subassemblies already discussed, a small amount of hardware is required during final receiver assembly. Basically, this hardware consists of nuts and bolts to attach the torus support ring and the aperture support ring to the bottom of the receiver casing. In addition, ceramic insulators and fastening nuts are required to attach the heat pipes to the heat pipe support ring. The hardware also includes weather protection for the insulation.

5.8 Receiver Assembly

The procedure employed in the fabrication of the heat pipe ABSR is outlined in Figure 5.2. This procedure is intended for use in the fabrication of a prototype receiver and would require significant changes for utilization in mass production. As illustrated in the figure, the assembly of several subsystems can be completed or nearly completed prior to final assembly of the receiver. This is true of the heat pipe assembly, the inlet and outlet plenum and duct assemblies, and the aperture assembly.

The heat pipe assembly is the most critical component of the receiver. The processing procedure shown in the figure assumes that iron is used as the buffer storage medium. It is also assumed that the heat pipe envelope with an integral air heat exchanger is obtained from an outside vendor. * Once the heat pipe envelope is received the wick structure is installed. At the same time, the iron storage capsule is machined to the proper dimensions. Then its surface is wicked and the standoffs are attached by welding. The capsule is inserted into the heat pipe envelope and the assembly is then cleaned. The heat pipe end caps and fill tube are welded to the assembly. Once the inlet and outlet header assemblies are fabricated, they are welded to the heat pipe to complete the assembly.

*One vendor capable of supplying the heat pipe-heat exchanger piece part is Tex-Fin Corporation of Houston, Texas.

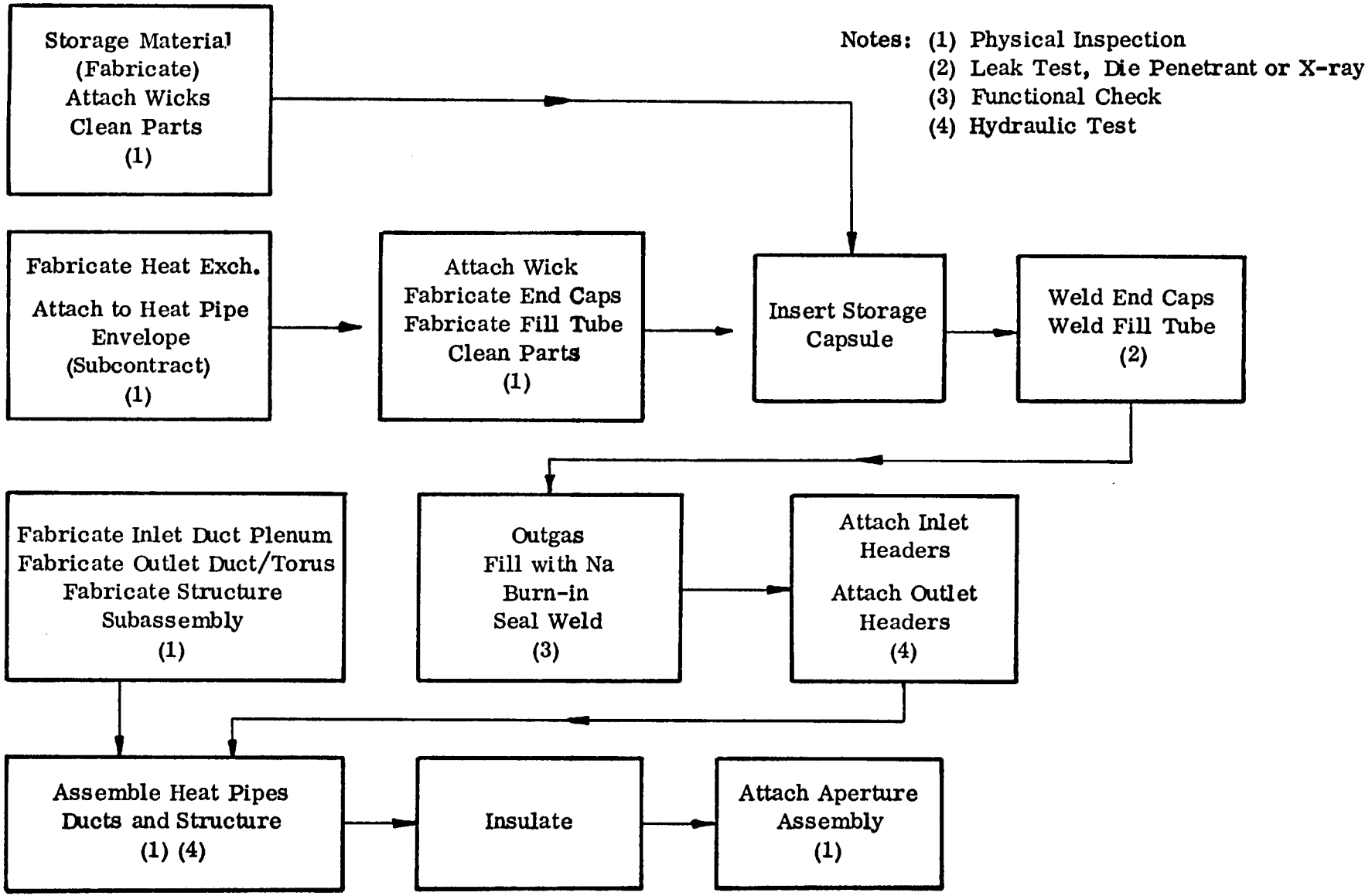

FIGURE 5.2

MANUFACTURING PROCESS

With the assembly completed, heat pipe processing continues with the installation of a high temperature valve to the fill tube. The assembly is helium leak checked and then outgassed under vacuum at high temperature (~1000°C) for several hours. The pipe is then charged by distilling a predetermined amount of sodium into the pipe. After charging, the heat pipe is cycled to a temperature slightly higher than the operating temperature to promote wetting of the wicked surfaces. Any noncondensibles are bled and then the fill tube is pinched and seal welded. At this point, the heat pipe is ready for any functional test prior to final receiver assembly.

The inlet plenum and duct can be fully assembled except for the cap. The inlet duct and cap cover plate are fabricated and then welded together. The flange is also attached to the duct prior to final receiver assembly. The exit plenum and duct can be fully assembled except for the outer torus surface. Fabrication of the subsystem includes drilling the lower torus surface and welding the locating pins, drilling the inner surface to interface with the heat pipes, and drilling the upper torus surface to accommodate the exit duct. These three surfaces are welded together and then the exit duct and flange are attached.

Once the subassembly fabrication is completed, final receiver assembly is initiated. The receiver casing is rolled and welded into cylindrical shape, and then the heat pipe support ring and the gusset reinforcement ring is welded in place. The upper heat pipe manifolds are inserted into the pre-drilled inlet plenum cap. The heat pipes are then fastened to the support ring and the manifolds are welded to the cap from the inside. The upper portion of the inlet plenum assembly is then welded to the cap. The torus-exit duct assembly is positioned and then welded to the lower heat pipe manifolds. The welding operation is done from the backside (inside the torus). The torus is then completed by installing and welding the outer surface. Then the receiver support ring and the gussets are welded to the receiver casing. The region above the inlet plenum is insulated and then the PCU mounting plate is attached to the casing. The region between the heat pipe heat exchangers and the casing is insulated, after which the aperture assembly is attached. Then the remainder of the receiver is insulated, starting with the torus and exit duct and ending with the outside of the receiver shell.

5.9 Stress Analysis

The solar receiver assembly was subjected to a stress analysis in accordance with Paragraph 9 of Exhibit I of the JPL specifications. The receiver meets these requirements including the ASME UPV Code, Section VIII, Division 1. A detailed analysis is available and Table 5.2 lists various items with the Margin of Safety available over allowable stresses.

The structural components were designed to allowable stresses of 2/3 of S_y at their respective operating temperature. Pressure loaded parts were analyzed in accordance to the ASME pressure vessel code which is based on 1/4 of S_{ult} at operating temperature. Stresses due to high ΔT's across the surface of the heat pipe were compared to 2/3 of S_y at the maximum operating temperature.

For all pressure parts, the margins of safety given in Table 5.2 convert to a minimum factor of safety of 4.35 based on ultimate strength. For all structural parts, the minimum factor of safety based on yield strength is 1.67. Since for most structural materials the yield strength is about 60% of ultimate, this converts to a factor of safety of 2.79 based on ultimate. The stress due to the temperature gradient in the heat pipe envelope has a factor of safety of 3.41 based on short-term yield and 3.83 based on short-term ultimate strength.

The analysis therefore shows that the solar receiver is reasonably safe and can be expected to endure moderate overloads which may occur in service.

PART	ITEM	Applied Load	% Margin of Safety	Analysis* Based On
Storage Capsule	Shell	36.75 psig	8.8	A-UG 31
	End Caps	36.75 psig	30.0	A-UG 34
Heat Pipe	Shell	22.0 psig	457	A-UG 27
	Shell	27.0°F	127	T-
	End Caps	22.0 psig	15.0	A-UG 34
Heat Exchanger	Heat Exchanger	22.0 psig	22.0	S-FP Stress
Inlet Plenum	Heads	22.0 psig	98.9	A-UG 32
	Head Weld	22.0 psig	Large	A-UG 27
	Reinforcement	22.0 psig	172	A-UG 40
Torus	Outer Cylinder	22.0 psig	12.9	A-
	Inner Cylinder	22.0 psig	42.4	A-UHA 28.1
	Top/Bottom Plates	22.0 psig	15.0	S-Bending

*A designates ASME Code, S designates Structural, T designates Thermal Stresses

TABLE 5.2

STRESS ANALYSIS SUMMARY

PART	ITEM	Applied Load	% Margin of Safety	Analysis* Based On
Structure	Attachment Flange	Bolt Loads	11.7	S-Bending
	Attachment Flange	Gusset Reaction	Large	S-Bending
	Gussets	Gusset Reaction Horizontal	Large	S-Bending
	Gussets	Gusset Reaction Vertical	Large	S-Bending
	Gussets	Gusset Reaction Vertical	249	S-Bending
	Cylinder Reinforcement	Gusset Reaction Vertical	76.2	S-Radial
	Cylinder Structure	Gravity & Wind	Large	S-Earthquake
	Equipment Mounting Plate	Gravity & Wind	Large	S-Bending
	Equipment Mounting Plate	Gravity & Wind	Large	S-Combined Bend Stress
	Heat Pipe Mounting Ring	Gravity & Wind	18.2	S-Bending

*A designates ASME Code, S designates Structural, T designates Thermal Stresses

TABLE 5.2 (Cont'd)

STRESS ANALYSIS SUMMARY

6. TECHNOLOGY STATUS

The operation of this type of receiver is based on heat pipe technology, in particular on liquid metal heat pipes. The heat pipe technology is about 16 years old and is well established. During the early years of heat pipe development, applications were mostly restricted to aerospace systems and the production quantities and concomitantly the hardware experience was rather limited. During the last few years, however, several commercial and industrial applications have emerged; and today, perhaps, one quarter of a million heat pipes are in use. Most of these heat pipes are of the low temperature type and fabricated from aluminum, copper, or carbon steel. The preferred working fluids are ammonia and various refrigerants.

In the high temperature field, much less hardware experience is available, in spite of the fact that high temperature liquid metal heat pipes were historically among the first to be developed. One notable exception is Dynatherm's product line of Isothermal Furnace Liners. These annular potassium and sodium heat pipes are widely used in industrial, government, and university laboratories for isothermalizing tubular furnaces. Their sizes range from 3.5 cm to 12.5 cm diameter and from 15 to 150 cm in length. More than 600 of these liquid metal heat pipes are currently in use.

In any high temperature system, materials problems are always of concern. Examples of potential problems are corrosion resistance, compatibility with the working fluid, hydrogen embrittlement, stress corrosion, long-term creep and rupture strength, and low cycle fatigue. A heat pipe, which is a sealed system with small internal volume and which contains a wick, may conceivably pose some additional problems. Among them are generation of noncondensible gas which is trapped within the pipe, the unusually large surface area exposed by the wick, and mass transport phenomena within the wick. These potential problems with high performance liquid metal heat pipes have been of some concern and may have been responsible for the slow acceptance of these devices. A systematic study of the various effects which might influence the reliability of liquid metal heat pipes was recently undertaken by GE for JPL.* The study showed that the applicable materials and liquid metal technology is

*Heat Pipe Operating Reliability for the Dish-Stirling Solar Receiver," by W. F. Zimmerman, General Electric Company, and J. W. Stearns, JPL. November 15, 1978.

well founded and that liquid metal heat pipes can be highly reliable devices. Also, the vast amount of liquid metal technology which has been developed during various reactor programs is directly applicable to the material problems in heat pipes. Highlights of the liquid metal and heat pipe background are:

- 800,000 hours cumulative testing of liquid metal systems during reactor programs at 800-2000°F (austenitic SS, cobalt, and nickel based alloys).
- 100,000 hours cumulative testing of sodium heat pipes reported in the literature through 1972 (1300-1500°F).
- 1,000,000 hours cumulative industrial use of Dynatherm's Isothermal Furnace Liners with 40,000 MTBF (900-2000°F).

Another concern which is frequently expressed about liquid metal heat pipes is their safety. Alkali metals are, of course, highly reactive with oxygen and with water. Unlike pumped liquid metal transport systems which contain large quantities of it, heat pipes usually contain only a very small amount of fluid. A typical sodium heat pipe, such as the ones designed for the ABSR, has a fluid inventory of only 77 g. Laboratory experiments at Dynatherm during which sodium and potassium heat pipes were made to fail at high temperatures have never lead to any violent reaction but always to a slow oxidation of the working fluid. The same observation was made by users of Isothermal Furnace Liners who exceeded the specified temperature limit due to a failure of the furnace control mechanism.

The technology of eutectic salt storage is not as well developed as the liquid metal heat pipe technology. Research by the Air Force has established that lithium salts and Inconel 617 are thermodynamically compatible up to 1225°C. Compatibility tests at 760°C were successful for at least 2000 hours and possibly for as long as 10,000 hours. Lithium fluoride salt has also been tested extensively in Cb-1Zr container capsules. While the tests were successful at least for the test duration of 5000 hours, Cb-1Zr is too expensive to be considered for a low cost solar collector. Dynatherm has conducted some compatibility testing with lithium bromide in Inconel 601 containers at 1200°C. For the duration of the tests (a few hundred hours), this combination was also found compatible. From the foregoing, it is apparent that fluoride salt storage systems look

promising but needs more long-term testing.

The thermal and mechanical design of the receiver has been based on established engineering principles. Radiation and convection heat transfer and mechanical stress calculations are straightforward. The low alloy steel used for the inlet duct and plenum has an allowable code stress of 5000 psi at 1050°F. Type 304 S/S at 1500°F has an allowable stress of 1400 psi. The pressure stresses in the heat pipe due to the vapor pressure are negligible. The dominant stresses in the heat pipe are the pseudo stresses resulting from the temperature gradient through the wall. They could conceivably lead to low cycle fatigue failure. An accurate analysis of these stresses would require a finite element analysis which was beyond the scope of the Phase 1 program. However, in the absence of pressure stresses, the short-term yield strength is a good approximation for the allowable temperature stress. At the nominal wall temperature of 1620°F, the yield strength of 310 S/S is 17,000 psi and the temperature induced stress is 5200 psi.

The hydrodynamic design of the heat pipe poses no special problems. Its performance was analyzed for nominal and off design conditions with respect to fluid transport, vapor dynamics, evaporator heat fluxes, sensitivity to orientation, and start-up phenomena. The performance was judged satisfactory, although additional analysis will be required prior to prototype fabrication.

7. TESTING REQUIREMENTS

A typical test program for the ABSR is outlined in Table 7.1. It consists of development tests on a component level, a bench test of the first prototype receiver, and acceptance tests of components and subsequent ABSR's. Each of these tests is described in the following subsections.

7.1 Heat Pipe Capability Test

The purpose of this development test is to verify that the heat pipe design is adequate for the required heat flux, heat throughput, and operating temperature at design and off-design conditions. The test setup is shown in Figure 7.1. Since it is difficult to simulate the circumferentially nonuniform heat input quantitatively, a separate condenser section with a calorimeter will be attached to the heat pipe as shown in the figure. Heat will be applied with a properly shaped RF coil in order to simulate the axial nonuniformity. Tests will be conducted at various evaporator heat fluxes, various total heat inputs, and operating temperatures. The heat pipe will also be tilted in order to evaluate performance at different receiver orientations. Another test will consist of start-up at various rates including a start-up with frozen sodium.

7.2 Heat Pipe/Heat Exchanger Test

The purpose of this test is to verify the performance of this subassembly and to establish acceptance criteria for the ABSR. The test setup is shown in Figure 7.2. Preheated air at atmospheric pressure will be passed through the heat exchanger. The test results will then be extrapolated to the design pressure of 36 psia. For this test, the heat will be applied with radiant heaters at approximately the same spatial distribution as in the receiver. This is important in order to simulate thermal stresses in the system. The tests to be conducted will include heat pipe performance (ΔT's), pressure drops, and heat exchanger performance (ΔT's) at various thermal inputs. Buffer storage performance and start-up will also be evaluated. Following the flow tests at ambient pressure, the heat exchanger will be pressurized and temperature tested.

TABLE 7.1

OUTLINE OF TEST PROGRAM

1. Heat Pipe Capability Test (Development)

Use single modified heat pipe

Test for:
- heat flux
- heat transport
- maximum temperature
- sensitivity to orientation
- start-up

2. Heat Pipe/Heat Exchanger Test (Development)

Use single module

Use preheated air at atmospheric pressure

Test for:
- heat pipe performance
- pressure drop
- gas temperature rise
- thermal resistance

Perform static pressure test at design temperature

3. Life Test (Development)

Use heat pipe/heat exchanger module

Operate at design temperature and pressure

Cycle daily

Continue for duration of program

TABLE 7.1 (Cont'd)

OUTLINE OF TEST PROGRAM

4. Receiver Bench Test (Prototype)

Use preheated pressurized air

Perform: static pressure test (cold)

static pressure test (hot)

no flow thermal efficiency test

thermal performance test at:
- 50% load
- 75% load
- 100% load
- 120% load

transient start-up and shut-down test buffer storage test

5. Acceptance Test (Each Heat Pipe)

Functional check at maximum and minimum operating temperature

6. Acceptance Test (Each Heat Pipe/Heat Exchanger Module)

Cold static pressure test

Static pressure test at operating temperature

7. Receiver Acceptance Test

Cold static pressure test

Cold flow test

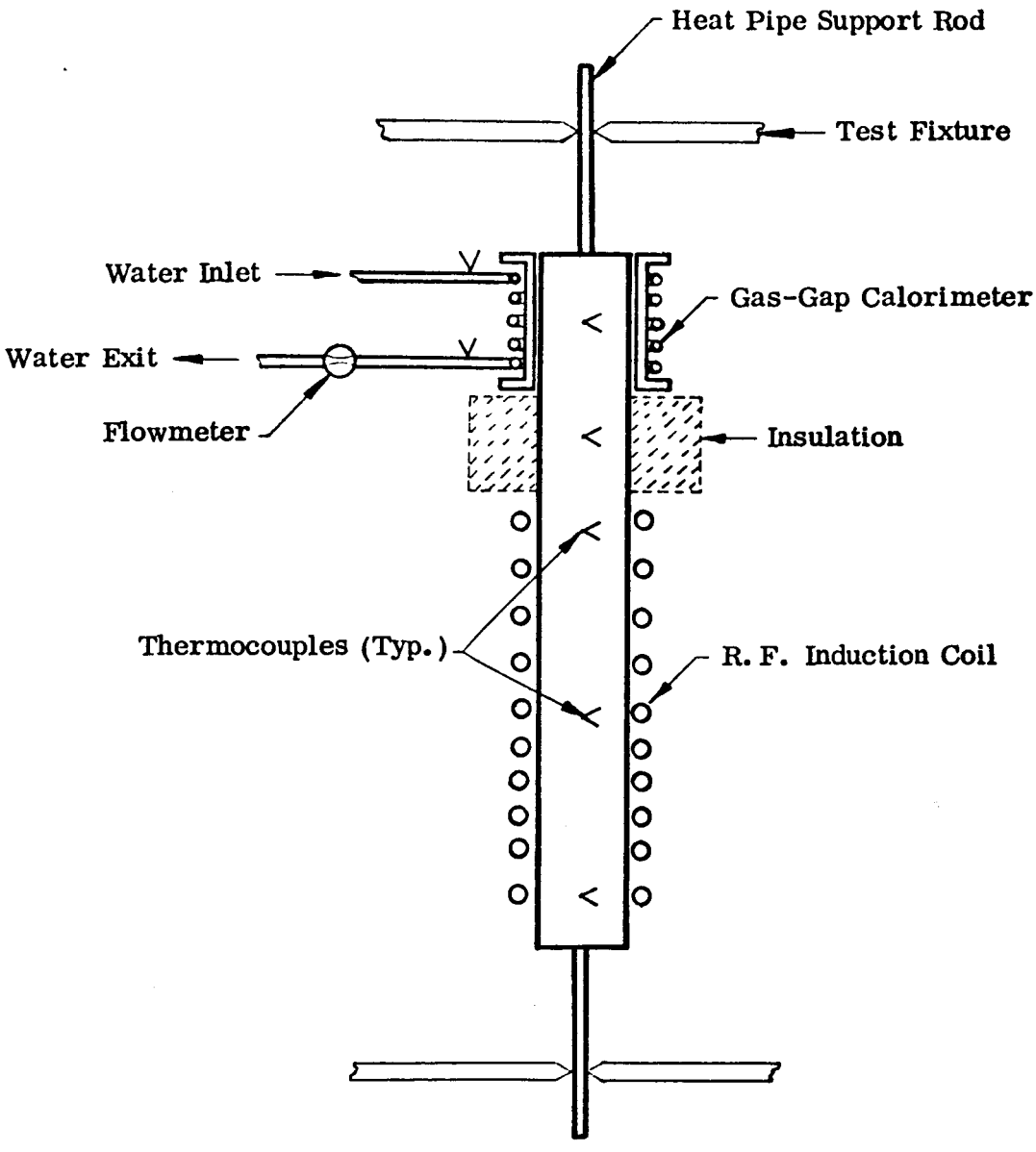

FIGURE 7.1

HEAT PIPE PERFORMANCE TEST SETUP

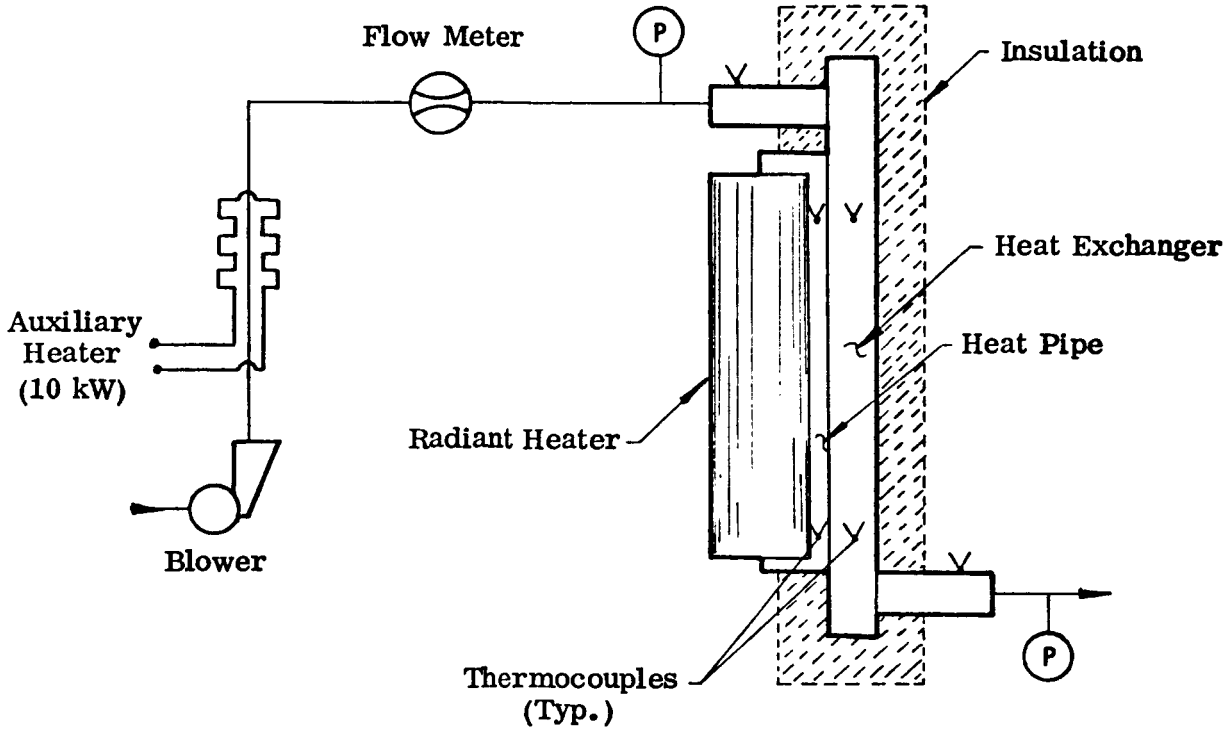

FIGURE 7.2

HEAT PIPE/HEAT EXCHANGER TEST SETUP

7.3 Life Test

The same heat pipe/heat exchanger assembly tested under (2) above will be life tested for the remainder of the program. The life test will be conducted with the heat exchanger pressurized statically and with sufficient heat input to maintain design operating temperature. Heat input and pressure will be cycled daily.

7.4 Receiver Bench Test

A full thermal performance test will be conducted on the first prototype receiver. The test loop which will be used for these tests is shown schematically in Figure 7.3. The heat input will be provided by a specially designed radiant heater, shown in Figure 7.4. It will use GE Type RH4204 quartz heater tubes. The tubes will be mounted around a water cooled stainless steel reflector. The reflector will be separated from the coolant by a thermal barrier (gas gap) in order to reduce heat losses. The heater will be installed in the cavity by removing the aperture assembly temporarily. During operation, the cavity will be flooded with nitrogen gas in order to allow the reflector to operate at elevated temperature without oxidizing. Compressed air will be provided by a 250 HP gasoline powered compressor. An air-to-air heat exchanger will recover about 65% of the input to the receiver and preheat the inlet air. An auxiliary heater and a bypass of the heat exchanger will give flexibility in selecting the receiver inlet temperature. The auxiliary heater will also be used during start-up. Both heaters will be powered with single phase, 480 V AC and the input will be varied in steps from 10% to 120% of design power. Gas flow will be controlled with pressure regulators and bypass valves and measured with an orifice type flow meter. The cooling water flow will also be regulated and monitored.

The receiver will be instrumented with high temperature thermocouples to measure temperatures at key locations. Temperature measurements on the heat pipe assembly will be made on the evaporator surface, vapor temperatures, and several locations on the heat exchanger surface. Temperatures on the inside and outside of the various insulation blankets will also be measured. Other instrumentation will include air and water flow measurement, absolute air pressure upstream

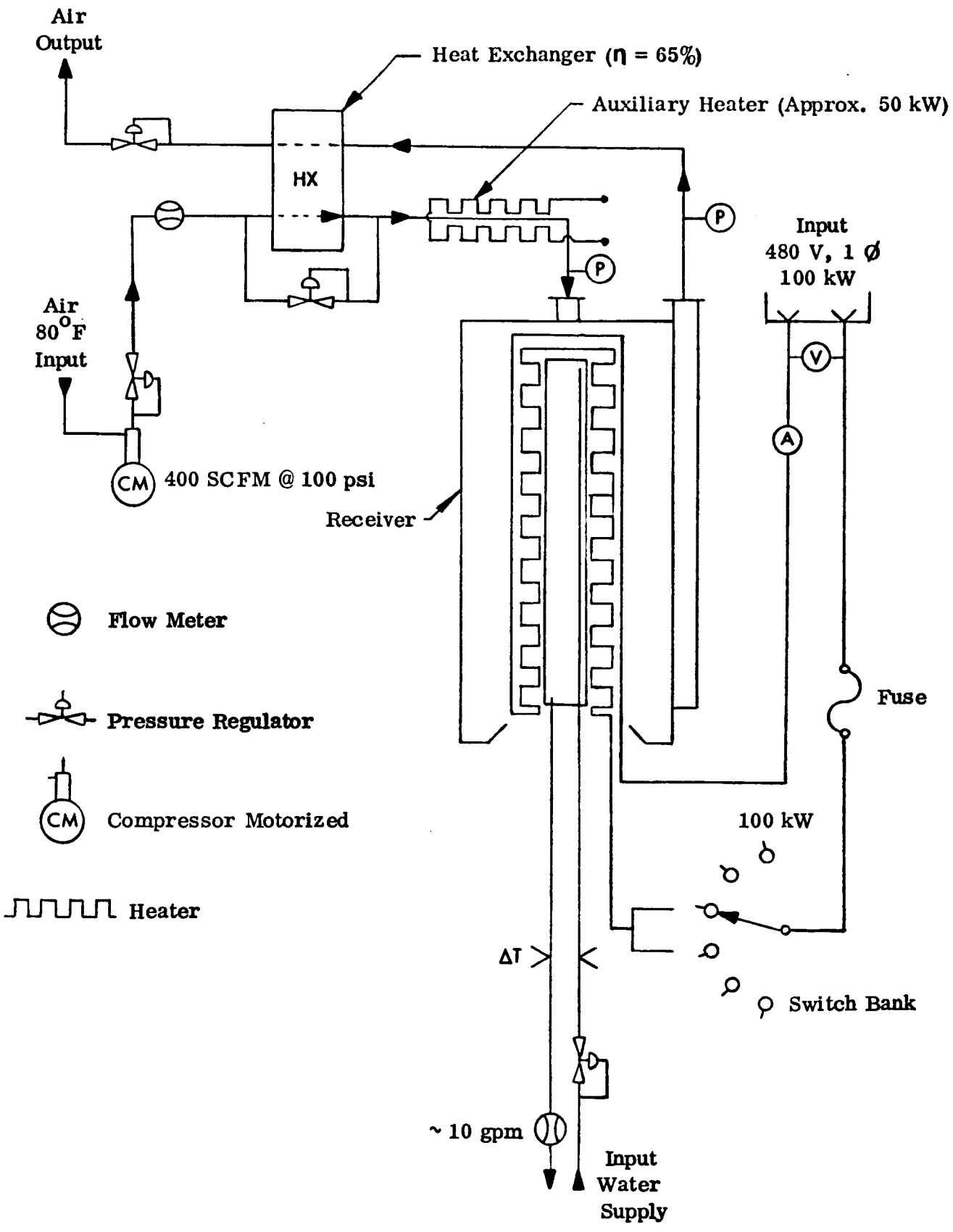

FIGURE 7.3

ABSR BENCH TEST SETUP

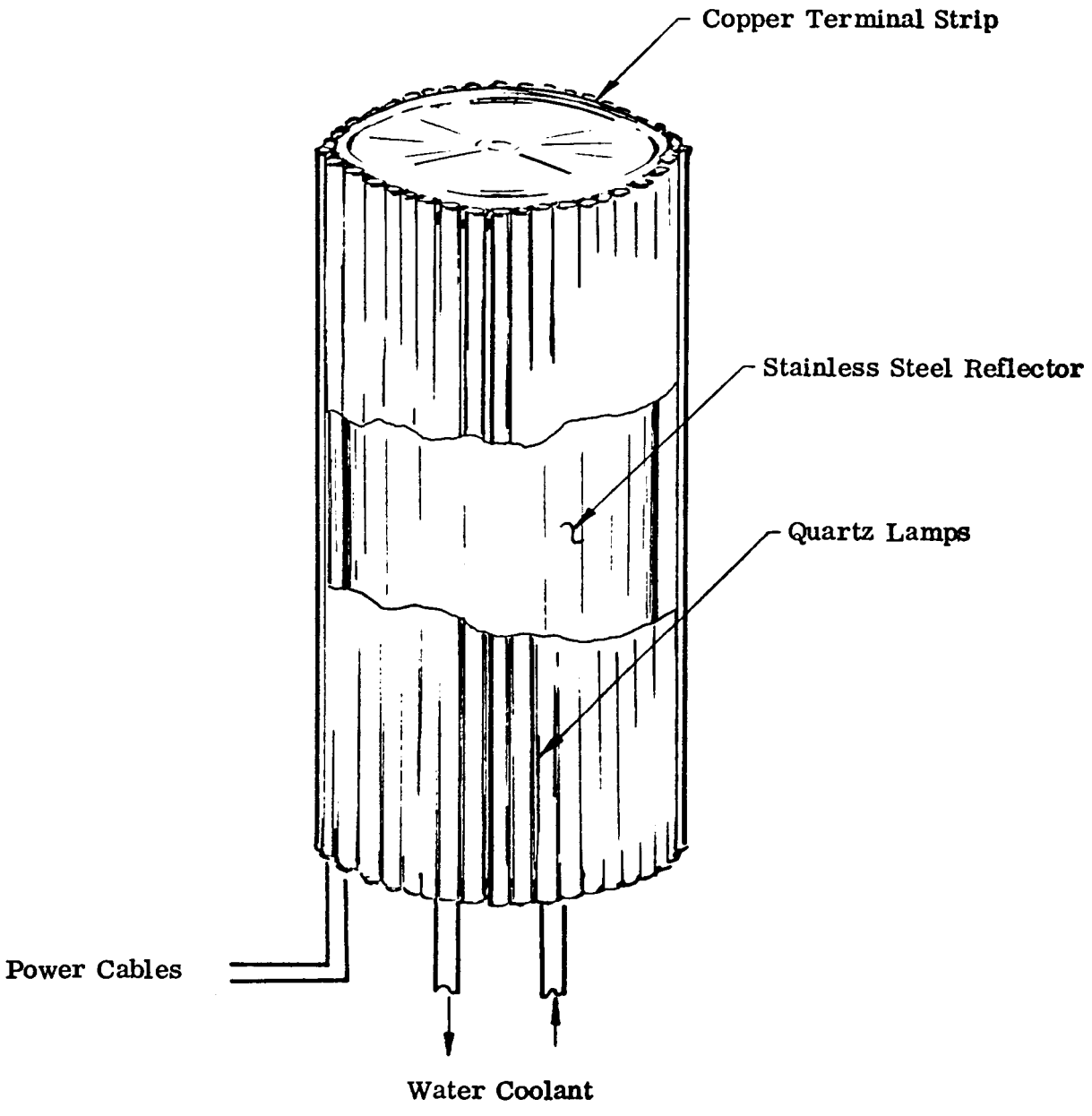

FIGURE 7.4

RADIANT HEATER FOR ABSR TESTS

and downstream of the receiver, electrical input, and cooling water temperature rise. Analog signals from all instrumentation will be transmitted to a 60 channel Doric Data Logger and simultaneously be processed on a HP 9835 A Desktop Computer.

A tentative outline of the tests to be conducted is listed in Table 7.1

7.5 Acceptance Tests

Each individual heat pipe and each heat pipe/heat exchanger module will be subjected to the acceptance tests listed under Items 5 and 6 of Table 7.1. Because of the high cost associated with performance testing of complete receivers, any receiver after the initial prototype will only be subjected to the acceptance tests listed in Item 7 of Table 7.1.

8. COST ESTIMATES

One objective of the study was to provide an initial evaluation of the mass producibility of ABSR's at a continuing annual rate of 100, 1,000, 10,000, 100,000 and 1,000,000 units. The mass production methods for key components and the major capital investment to achieve mass production need also to be identified.

It is obvious that quantity production will have a great and beneficial impact on the cost of the receiver. However, in order to apply mass production techniques, the receiver will have to be completely redesigned from the current prototype. Since high temperature heat pipes have not been mass produced to date, such an extrapolation is somewhat risky and should be deferred until after the development of a prototype. Nevertheless, several approaches of estimating production costs in large quantities have been considered and are outlined below.

The general approach which was taken for estimating receiver cost at various production rates is as follows. For prototype quantities (one to three units), the detailed assembly drawings which were prepared during the study provide a fairly firm basis for a cost estimate. For small quantity productions (i.e., 100 units annually), the same basic design was considered but with some modifications for easier fabricability. Also, an improved and simplified heat pipe fabrication process was assumed for these moderate quantities. Since heat pipe processing currently is the most labor intensive part of the receiver fabrication, an improvement in this area has a significant impact on overall cost. For very large quantities (10,000 or more units annually), a complete redesign of the receiver is appropriate. One approach to a mass producible design is shown schematically in Figure 8.1. The entire heat pipe/heat exchanger assembly would be fabricated like a panel coil heat exchanger using seam welding techniques. Inlet and outlet headers for the gas are made an integral part of the assembly. In this concept, the heat pipes are still individual vapor chambers so that draining of the fluid in a gravity field is avoided. Initial discussions with a leading manufacturer of such coils have established, in principle, the feasibility of this approach.

A breakdown of labor and material costs for prototypes and for small quanti-

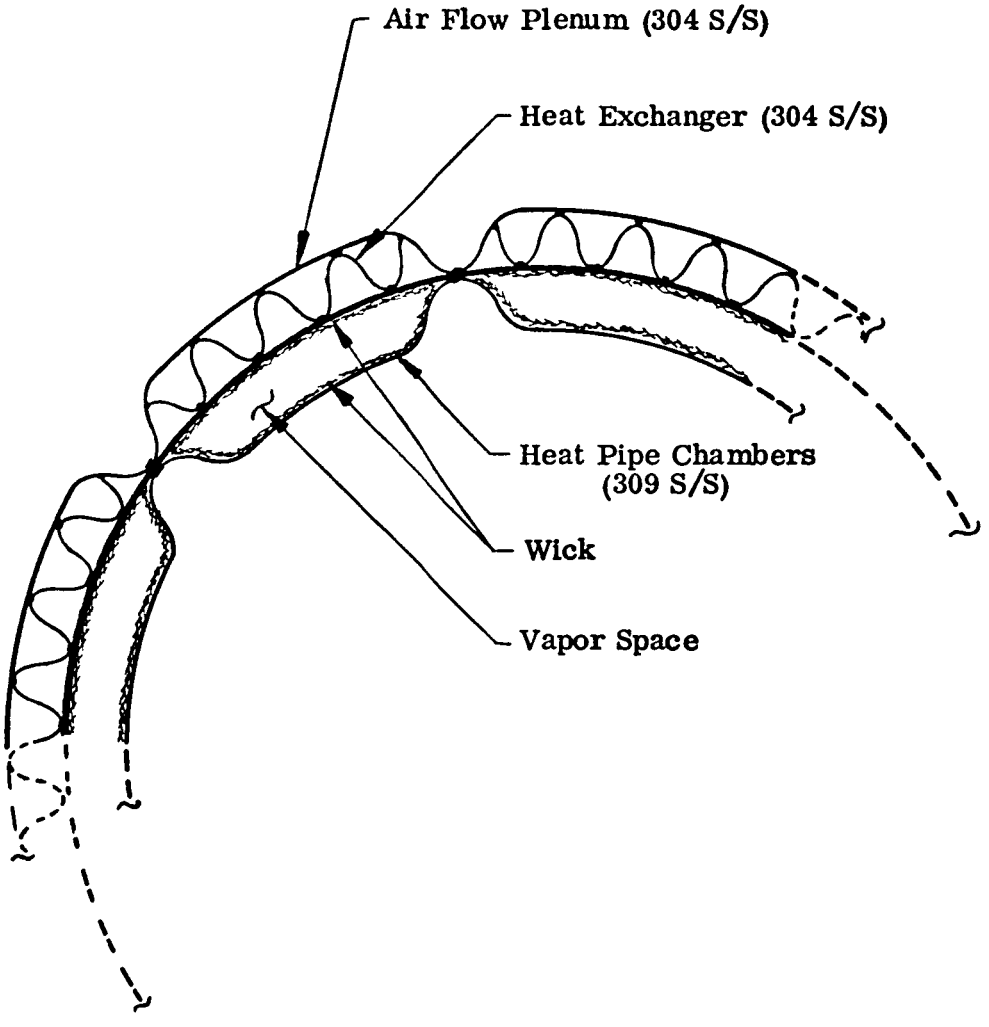

FIGURE 8.1

CONCEPT OF INTEGRATED HEAT PIPE-HEAT EXCHANGER

ties (~100) is given in Table 8.1. The labor hours are estimates obtained from our manufacturing department and do not include engineering support or testing.

The large difference in labor between the prototype and the production of 100 units comes from the different assumption for heat pipe processing. The heat pipe manufacturing process is well established but is currently performed entirely in the laboratory. For one or a few prototypes, this established process would be applied. The major time consuming element is that each heat pipe is processed individually. Table 8.2 shows a comparison between the current process and a proposed production process for small quantities. It is expected to decrease labor input by a factor of 10. While the production process retains all the proven elements, heat pipes would be processed in batches of 20 instead of individually. The major development required is the design and acquisition of the equipment needed to implement this process.

Another striking difference between prototype and 100 units is the material cost for the heat pipe subassembly. This difference is somewhat misleading since a large fraction of the cost consists of a subcontract for attaching the heat exchanger to the heat pipes. The quoted price for the heat exchanger (including material for the heat pipe envelope and the fins) is $4,260 for prototypes and $1,160 for quantities of 100. Obviously, the price for the prototypes includes a large ount of tooling. Other differences between prototypes and 100 units shown in Table 8.1 are the result of selecting more cost effective manufacturing techniques for the larger quantities (e.g., substitute stamping for machining).

The trend of true material cost as a function of quantity is shown in Figure 8.2. Here the same basic design was assumed even for very large quantities of 10,000 or more annually.

Estimates of overall production costs were also made. For prototype and quantities of 100, the data shown in Table 8.1 were used with some provisions for tooling ($3,945 for prototype and $7,200 prorated to 100 units), contingency (20% for prototype only), and engineering support (20% for prototype only). Burdened labor costs of $15.34 were used for manufacturing labor, $25.00 for engineering labor, and a material burden factor of 1.24. The results are shown in Table 8.3.

SUBASSEMBLY	Labor Hours		Material Dollars	
	Prototype	Quantity 100	Prototype	Quantity 100
1. Heat Pipe/Heat Exchanger/Buffer Storage	312.0	52.0	4988	1718
2. Inlet Duct/Plenum	22.5	0.5	243	192
3. Exit Duct/Torus	39.0	4.3	909	267
4. Aperture	15.0	3.3	67	57
5. Structure	48.0	4.4	298	207
6. Insulation	9.0	6.0	136	109
7. Hardware	--	--	14	12
Assembly	150.0	36.0	--	--
TOTAL	595.5	106.5	6655	2562

TABLE 8.1

LABOR AND MATERIAL COST FOR
PROTOTYPES AND SMALL QUANTITIES

TABLE 8.2

HEAT PIPE MANUFACTURING PROCESS

LABORATORY PROCESS (Individual Heat Pipe)	PRODUCTION PROCESS (Batches of 20 Heat Pipes)
Fabricate Parts	Fabricate Parts
Attach Wicks	Attach Wicks
Clean Parts	Clean Parts
Weld End Caps, Fill Tube	Weld One End Cap
Attach Valve	Outgas Parts
Outgas	Place in Dry Box
Distill Sodium into Heat Pipe	Fill with Liquid Sodium
Heat to Operating Temperature	Weld Second End Cap
Remove Noncondensible Gas	Attach Valve
Seal Weld	Remove from Dry Box
Functional Check at Operating Temperature	Evacuate
	Heat to Operating Temperature
	Remove Noncondensible Gas
	Seal Weld
	Functional Check at Operating Temperature

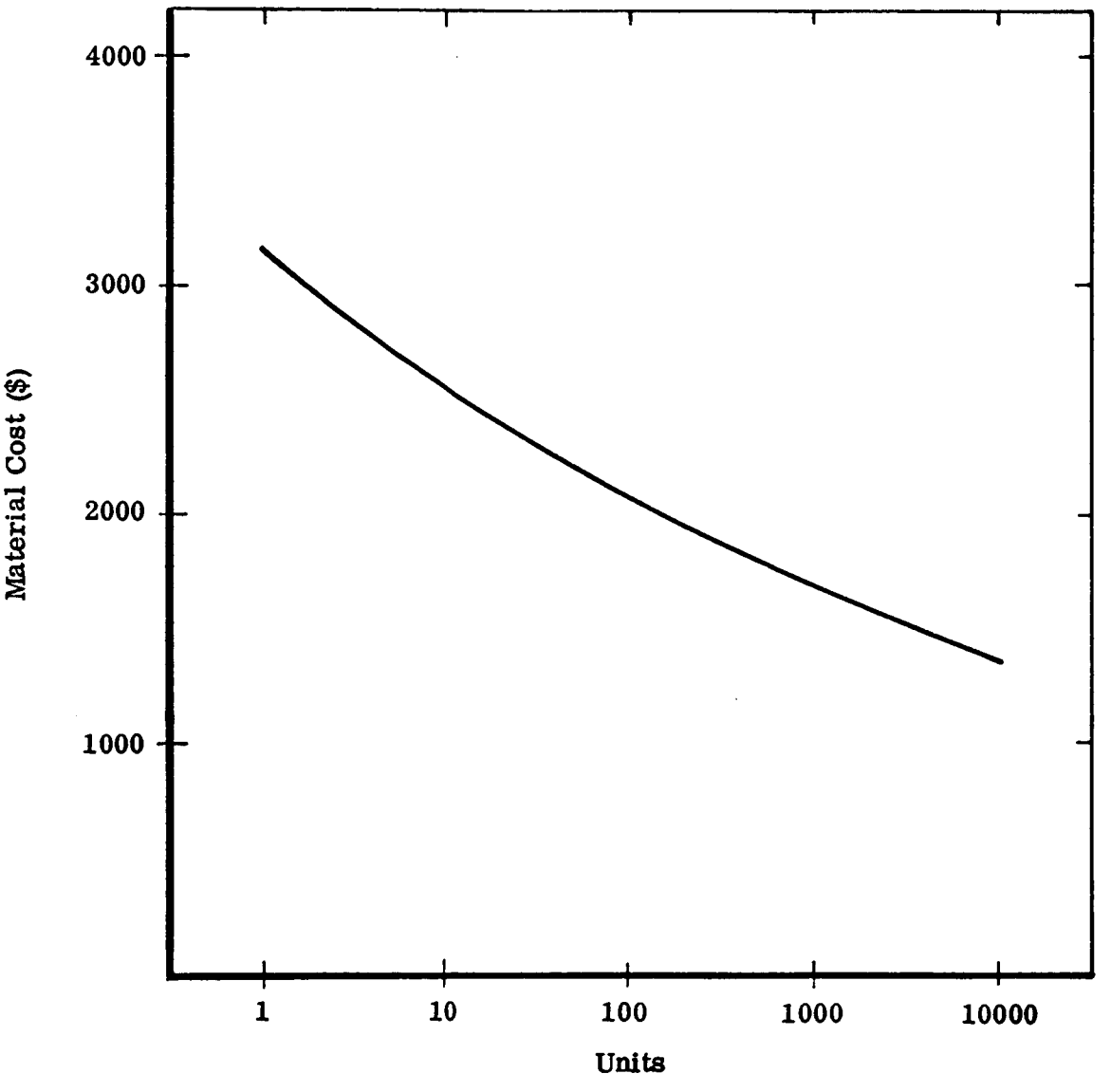

FIGURE 8.2

TREND OF MATERIAL COST

1st Prototype 2nd, 3rd Prototype	$27,097 with Fe Storage $17,676 with Fe Storage	$25,237 w/o Storage $16,156 w/o Storage
Annual Quantity of 100	$ 4,900 with Fe Storage	
Large Quantities (>10,000/year)	$1,100 - $2,640 (Range)	

TABLE 8.3

SUMMARY OF ESTIMATED FABRICATION COSTS

This table also gives an estimate for a second and third prototype with and without buffer storage.

The estimate for the large quantities are less well defined. The higher figure of the indicated range was obtained by using the material costs given in Figure 8.2 for 10,000 units and then adding a labor cost of $1.23 per pound weight of the receiver. This labor cost was extrapolated from the selling price of typical mechanical products and is, of course, only a very rough guess. The lower figure was obtained in a different way. It is based on a preliminary estimate of labor and material cost of the integrated heat pipe-heat exchanger shown in Figure 8.1. Added to this was then the cost of 250 pounds of supporting structure and insulation at a rate of $1.50 per pound of fabricated material. Although these estimates for large production quantities are only very rough at the present time, they show that a heat pipe ABSR has the potential of approaching the cost goals set by the JPL program.

The fabrication of one or several prototypes will not require any significant tooling. For the production of quantities of 100 or more, the heat pipe fabrication process needs to be revised as discussed earlier in this section. The cost of developing the alternate process should be of the order of $200,000. No attempt is made at this time to estimate the required capital investment for high volume production of the ABSR.